Escuela Agrícola Panamericana, Zamorano

Environmental Science and Development

B.S. in Environmental Science and Development

Special Graduation Project

Analysis of Land Use and Land Cover Changes on the Island of Roatán from 2017 to 2025

Nicholas Matthew McNab Tomé

Advisors

Alexandra Manueles, Mtr.

José Antonio Molina, M.Sc.

Honduras, august 2025

Authorities

KEITH ANDREW

President i.a.

ANA M. MAIER ACOSTA

Vice President and Academic Dean

VICTORIA CORTÉS MATAMOROS

Director of Environmental Science and Development

JULIO NAVARRO

Secretary General

Table of Contents

List of Tables

List of Figures

List of Appendices

Abstract

This study analyzes land use and land cover (LULC) changes on the island of Roatán, Honduras, between 2017 and 2025 using remote sensing and GIS-based techniques to categorize land use and quantify the gains, losses, and transitions related to shifting land use patterns associated with tourism and development pressures. Multi-temporal Sentinel-2A imagery was processed through supervised classification using the Random Forest algorithm, guided by training data corresponding to key macro land cover categories including vegetation, artificial surfaces, wetlands, open spaces, and water bodies. To complement the classification process, two spectral indices: NDVI and NDBI were applied as visual interpretation tools to support the identification of vegetation health, built-up density, and land transformation trends. This study employed a simplified Corine Land Cover (CLC)-inspired methodology, adapted to the tropical island context. Quantitative change analysis was conducted using the Pontius matrix to evaluate spatial gains, losses, and persistence across land cover classes. Results indicate a marked expansion of industrial, commercial and transport zones and a notable reduction in open areas with little or no vegetation, reflecting a trend toward intensified industrialization on Roatán. Forests showed both losses and localized gains, reflecting land use fluctuations. This research contributes to understanding the spatial development dynamics and environmental change in Roatán, with implications for land management, conservation planning, and future coastal resilience strategies.

Keywords: Land use and land cover change (LULC), NDBI, NDVI, Pontius matrix, remote sensing

Resumen

Este estudio analiza los cambios en el uso y la cobertura del suelo (LULC, por sus siglas en inglés) en la isla de Roatán, Honduras, entre 2017 y 2025, utilizando técnicas de teledetección y SIG para categorizar el uso del suelo y cuantificar las ganancias, pérdidas y transiciones relacionadas con los patrones cambiantes de uso asociados a las presiones del turismo y el desarrollo. Imágenes multitemporales del satélite Sentinel-2A fueron procesadas mediante clasificación supervisada utilizando el algoritmo Random Forest, guiada por datos de entrenamiento correspondientes a categorías macro clave de cobertura del suelo, incluyendo vegetación, superficies artificiales, humedales, espacios abiertos y cuerpos de agua. Para complementar el proceso de clasificación, se aplicaron dos índices espectrales: NDVI y NDBI, como herramientas de interpretación visual para apoyar la identificación del estado de salud de la vegetación, la densidad de áreas construidas y las tendencias de transformación del suelo. Este estudio empleó una metodología simplificada inspirada en Corine Land Cover (CLC), adaptada al contexto de una isla tropical. El análisis cuantitativo de cambios se realizó utilizando la matriz de Pontius para evaluar las ganancias, pérdidas y persistencia espacial entre clases de cobertura del suelo. Los resultados indican una marcada expansión de las zonas industriales, comerciales y de transporte, así como una reducción notable de las áreas abiertas con poca o ninguna vegetación, lo que refleja una tendencia hacia una industrialización intensificada en Roatán. Los bosques mostraron tanto pérdidas como ganancias localizadas, reflejando fluctuaciones en el uso del suelo. Esta investigación contribuye a la comprensión de las dinámicas de desarrollo espacial y cambio ambiental en Roatán, con implicaciones para la gestión del territorio, la planificación de la conservación y futuras estrategias de resiliencia costera.

Palabras clave: Matriz de Pontius, NDBI, NDVI, sensores remotos, transformación del suelo, uso y cobertura del suelo (LULC)

Introduction

Island ecosystems are highly vulnerable to land use/cover changes (LULC) due to their limited space and fragile biodiversity (Tuholske et al., 2017). Roatán, the largest of the Bay Islands of Honduras, has experienced significant LULC transformations driven by rapid urbanization, tourism expansion, and demographic growth. These pressures have led to deforestation, loss of mangroves, and degradation of coastal habitats, impacting both the environment and local communities. Understanding the magnitude and trends of these changes is essential for sustainable land management and decision-making.

To acknowledge the human dimensions of global change, the International Geosphere-Biosphere Program (IGBP) and the International Human Dimensions Program (IHDP) initiated the "Land Use/Cover Change (LUCC)" project in 1995 (Guan et al., 2011). One of the most effective methods for assessing LULC changes is remote sensing, which utilizes satellite imagery to monitor and analyze environmental transformations over time. This technology has become increasingly valuable for detecting land cover shifts, quantifying deforestation, and assessing urban expansion. Accurate and up-to-date land use and land cover (LULC) maps are essential for numerous applications, including urban and regional planning, disaster and hazard monitoring, natural resource and environmental management, and ensuring food security (Zhang & Li, 2022). Modern satellite missions such as Landsat and Sentinel provide high-resolution, multi-temporal data that enable detailed change detection analyses, supporting long-term environmental monitoring efforts. Satellite imagery has become a crucial tool for observing and analyzing transformations in both natural landscapes and human-made environments (Hemati et al., 2021).

Roatán has diverse topography and ecosystems, ranging from forested highlands to coastal mangroves and wetlands. A ridge runs along the island's center, reaching a maximum elevation of 244 m, with rock formations composed of serpentinite, amphibolite, biotite, chlorite schist, and gneiss (McBirney & Bass, 1969; Sutton, 2015). The northwestern coastline features rocky outcrops, alluvial

deposits, and limestone formations, while several natural and artificial beaches line the island's shores (Sutton, 2015). Tuholske et al., 2017 documented significant tourism-related land cover changes on Roatán over a 30-year period, identifying substantial habitat loss driven by development pressures. Their results indicate that urban area increased by 982.8 ha (227.7%), with 224.1 ha (19.1%) of mangroves being converted to urban land. This study highlighted the extent of environmental transformation associated with tourism growth; however, its temporal scope ended in 2015, leaving a critical gap in understanding more recent land use and land cover (LULC) dynamics on the island. There is an urgent need for updated data to inform land management strategies.

A periodic assessment of LULC changes is essential for informed decision-making. Forested land use is associated with better coral health indicators, whereas human-driven land uses such as urbanization and agriculture contribute to reductions in coral cover, species diversity, colony size, and structural complexity. (Carlson et al., 2019). The rapid tourism explosion since the 1990s of over 2.41 million tourists in 2024, according to the Roatan Tourism Bureau (2024), which has driven infrastructure development, calling for regular monitoring of land cover changes. The findings of this study could be valuable for policymakers, municipal authorities, and local organizations such as ZOLITUR (Zona libre turistica islas de la bahia), RTMP (Roatan marine park), and BICA (Bay islands conservation agency), aiding in sustainable planning and conservation efforts.

This research aims to analyze land use and land cover (LULC) changes on Roatán from 2017 to 2025 using remote sensing and geo graphical information-based techniques, which constitutes the general objective of the study. To achieve this, the study seeks to classify and quantify land cover changes; specifically gains, losses, and transitions between categories—through supervised classification and change detection analysis using multi-temporal satellite imagery. Additionally, it aims to identify which land cover categories experienced the greatest increases and decreases in area over the study period, providing a clearer understanding of the spatial dynamics and land transformation trends on the island.

Methodology

Study Area

Roatán, the largest of Honduras's Bay Islands, located in the Caribbean Sea, approximately 60 km north of mainland Honduras. It extends about 59 km in length and 8 km at its widest point, covering an area of approximately 130 km². The island is part of the Mesoamerican Reef System (MAR), the largest coral reef system in the Western Hemisphere, which stretches over 1,000 km from Mexico to Honduras. Recognized as a United Nations Educational, Scientific and Cultural world heritage site, the MAR plays a vital role in coastal protection, marine biodiversity, and local fisheries, while also serving as a key attraction for the island's growing tourism industry (Burke & Maidens, 2004; Mcfield et al., 2018). However, coastal development, deforestation, and pollution increasingly threaten this delicate marine ecosystem.

Roatán has a tropical climate, receiving an average annual rainfall of 2,000 mm. The rainy season occurs from October to November, while the dry season (January to June) sees significantly lower precipitation, often below 100 mm. Rainfall distribution varies, with the eastern part of the island receiving less precipitation than the west, leading to drier vegetation types, such as mixed shrubs and grasslands (Stonich, 1998; Tomczyk, 2010).

Administratively, Roatán is divided into two municipalities, Roatan and José Santos Guardiola, each with distinct land use patterns (Figure 1).

Figure 1

Roatán Island map with municipal boundaries

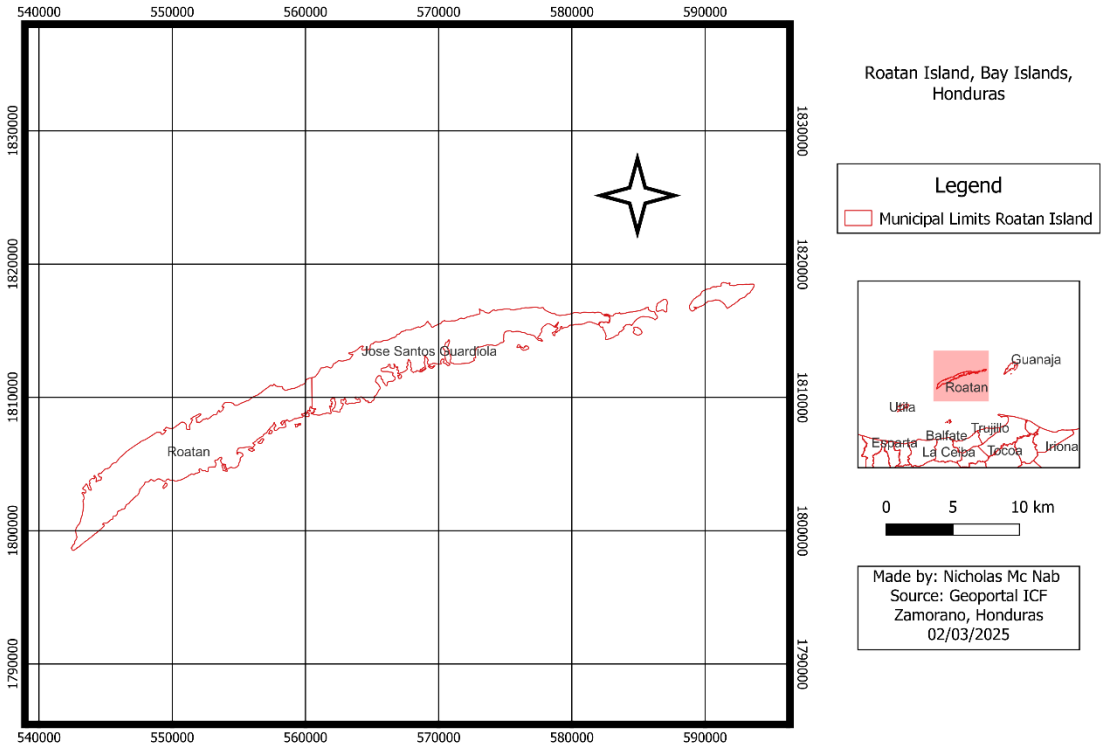

Note. Own elaboration based on geoportal data (Instituto de Conservacion Forestal, n.d).

Roatán Municipality (Western Region)

The western region has experienced significant urban expansion, largely due to tourism-driven infrastructure projects. This area is home to the Roatán International Airport and two major cruise ship terminals—Port of Roatán and Mahogany Bay—which have contributed to rapid land conversion from natural habitats to urbanized areas (Tuholske et al., 2017). Major population centers such as Coxen Hole, French Harbour, and West End have seen substantial increases in commercial and residential development, often at the expense of forests, wetlands, and mangrove ecosystems (Stonich, 1998).

José Santos Guardiola Municipality (Eastern Region)

In contrast, the eastern municipality of José Santos Guardiola remains less urbanized, with lower population density and greater ecological conservation efforts. This region contains several protected areas, including Port Royal National Park, which supports biodiversity conservation and

sustainable land management (Tomczyk, 2010). Additionally, Santa Elena Wetland System recognized as a RAMSAR (Convention of wetlands) site in 2018 (1,542.8 ha) helps safeguard mangroves and marine habitats. While small urban centers such as Oak Ridge and Punta Gorda have grown modestly, land conversion has been much slower compared to the western region.

Study Design

This is a descriptive, non-experimental, and longitudinal study. It is a descriptive study because the analysis focuses on classifying, describing, and comparing LULC changes in Roatán between 2017 and 2025. There is no manipulation of variables in a controlled setting, making it non-experimental. It is a longitudinal study as it examines LULC dynamics over two different time periods to assess changes over nearly a decade.

This study uses Sentinel-2A satellite imagery from the years 2017 and 2025 to analyze land use and land cover (LULC) changes in Roatán. A supervised classification approach will be employed to generate land cover maps using a simplified version of the CORINE Land Cover (CLC) methodology. This process will involve assigning land cover categories—such as urban areas, vegetation, and wetlands—based on manually selected training samples and spectral signatures.

In addition to supervised classification, a set of spectral indices will be applied to support visual interpretation of landscape dynamics. These indices do not constitute an unsupervised classification method but rather serve as analytical tools to highlight specific land cover features and facilitate a more intuitive understanding of spatial patterns. Specifically, the Normalized Difference Vegetation Index (NDVI) (Tucker, 1979) and the Normalized Difference Built-up Index (NDBI) (Zha et al., 2003), will be used to generate thematic maps that reveal vegetation health, urban density, and built-up distribution. In line with the main objective to categorize and classify the different land uses and land covers.

This combined use of supervised classification and index-based visualization enables a more comprehensive and nuanced analysis of land cover transformations across the study period. All image processing and spatial analysis will be carried out using QGIS 3.42.3®. A confusion matrix will be generated to assess the accuracy of the supervised classification results for each year. This matrix compares the predicted land cover classes from the classification output against a set of reference data, allowing for the identification of both correctly classified and misclassified area. Finally, the Pontius matrix will be used to quantify land cover change by estimating the spatial gains, losses, and transitions between land cover categories. For this study´s secondary objective to quantify and describe the trends exhibited from the LULC maps that have been generated from the main objective.

Spectral Index-Based Visual Analysis

In addition to the supervised classification performed using the Random Forest algorithm, this study employs spectral indices as complementary tools for interpreting land cover conditions and change patterns. These indexes are not used as unsupervised classification techniques, but rather as diagnostic visual layers that enhance the interpretation of thematic features such as vegetation health and built-up density, across the landscape. By applying targeted index formulas to Sentinel-2 imagery, it is possible to generate raster outputs that highlight specific land cover characteristics and support a clearer, more informed understanding of the transformations that occurred between 2017 and 2025.

The selected indexes; NDVI and NDBI are widely recognized in the remote sensing literature for their effectiveness in delineating vegetation, artificial surfaces, and mixed-use urban environments, respectively. Each index was computed using appropriate spectral bands from Sentinel-2 imagery and reclassified into descriptive value ranges. These outputs were used not as classification layers, but as visual interpretation tools to validate patterns, identify outliers, and complement the creation of training data for the supervised classification.

NDVI

The Normalized Difference Vegetation Index (NDVI) is one of the most fundamental and enduring remote sensing indices used to evaluate vegetative cover and condition. Originally developed by Tucker (1979), NDVI was designed to detect live green vegetation by exploiting the unique spectral reflectance properties of vegetation: strong absorption of red light due to chlorophyll and high reflectance in the near-infrared (NIR) spectrum due to the internal structure of healthy plant leaves. The NDVI formula is expressed in Equation 1.

$$NDVI = \frac{(NIR - Red)}{(NIR + Red)} \quad [1]$$

Tucker's pioneering study utilized satellite-derived radiance data to monitor vegetation dynamics in semi-arid regions of Senegal. His findings demonstrated that NDVI could reliably quantify vegetation biomass, phenology, and canopy structure over time, even in areas with low vegetation density. This marked the beginning of spectral index-driven remote sensing for land monitoring. More than four decades later, NDVI remains a central tool in land use and land cover (LULC) classification, due to its simplicity, robustness, and interpretability.

In the present study, NDVI was computed from Sentinel-2 imagery using Band 8 (NIR) and Band 4 (Red). Its application enabled a rapid and effective unsupervised classification of the study area into vegetation and non-vegetation zones, without the need for training data. The resulting NDVI raster was segmented into land cover categories based on value thresholds (Table 1), allowing differentiation of dense vegetation, sparse cover, and anthropogenic surfaces.

This approach is well-supported by recent literature. Da Silva et al. (2020) used NDVI to classify a complex rural landscape in southern Brazil, demonstrating high accuracy in distinguishing native forests, fallow land, and water bodies. Similarly, Sohail (2020) applied NDVI in the arid urban environment of Karachi, successfully mapping orchards, mangroves, and vegetation pockets. Akbar et

al. (2019) further operationalized NDVI thresholds for automatic classification of vegetation density in Pakistan's forested regions, providing a clear range of values for land cover interpretation.

The NDVI range classification used in this study is adapted from Akbar et al. (2019), as shown in Table 1.

Table 1

Classification of land cover according to NDVI values

NDVI Range	Land Cover Description
-0.28-0.015	Water
0.015 – 0.14	Artificial surfaces
0.14-0.27	Open spaces with little or no vegetation
0.27-0.36	Sparse vegetation
0.36-0.74	Dense vegetation

Note. Adapted from Akbar et al. (2019)

NDBI

The Normalized Difference Built-up Index (NDBI) was first proposed by Zha et al. (2003), as a simple yet effective method for identifying built-up areas in satellite imagery, especially in rapidly urbanizing environments. The index utilizes the spectral properties of urban materials, which tend to reflect strongly in the short-wave infrared (SWIR) region and less in the near infrared (NIR), a pattern opposite to that of vegetation. The NDBI is calculated using Equation 2.

$$\text{NDBI} = \frac{(\text{SWIR} - \text{NIR})}{(\text{SWIR} + \text{NIR})} \quad [2]$$

In this study, NDBI was derived from Sentinel-2 imagery using Band 11 (SWIR) and Band 8 (NIR). This index was chosen to isolate and classify built-up areas such as residential, commercial, and transportation infrastructure without the need for ground-truth data or training samples. The index values typically range between -1 and +1, where positive values generally indicate urban surfaces and negative values correspond to vegetation or water (Table 2).

Table 2

Land cover classification based on NDBI values

NDBI Range	Land Cover Description
< 0.00	Vegetation or water
0.00 – 0.20	Transitional surfaces
> 0.20	Built-up / urban features

Note. Adapted from Zha et al. (2003)

Supervised Land Use and Cover Classification

A supervised classification method was applied, utilizing a simplified version of the Corine Land Cover (European Environment Agency, 2019), methodology to categorize different land cover types such as vegetation, urban areas, water bodies, and wetlands. The classification accuracy will be evaluated using a confusion matrix, which compares classified results with reference data to assess errors of commission and omission. Change detection analysis will then be performed by comparing classified maps from both years, allowing for the identification of land cover trends such as deforestation, urban expansion, or mangrove loss.

The process begins with a pre-processing phase and concludes with a post-processing phase (Fig. 2). This approach has been widely used in similar studies, demonstrating its effectiveness in monitoring environmental changes and supporting sustainable land management strategies (Alqurashi & Kumar, 2013).

Figure 2

Data collection and processing flowchart

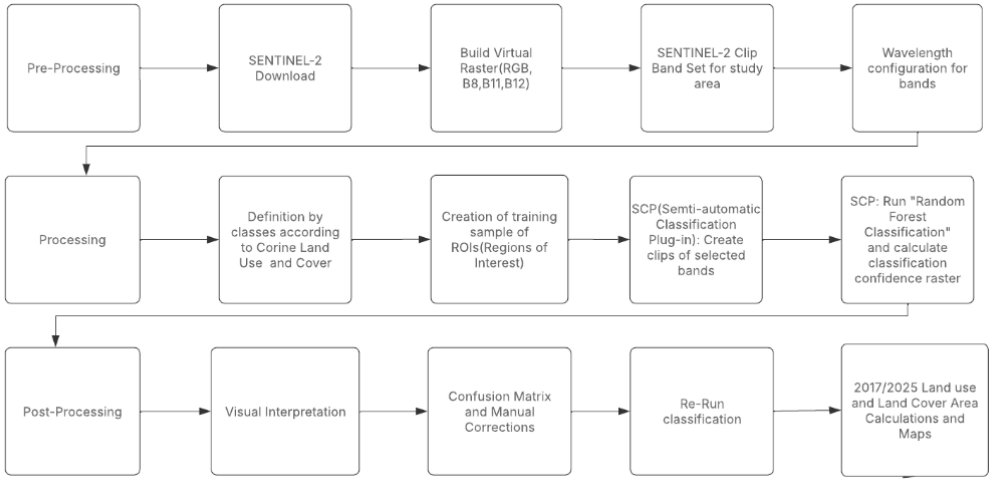

Note. Own elaboration based on supervised classification workflow using and Sentinel-2 imagery.

Pre-processing phase of Supervised classification of LULC Maps

The pre-processing phase ensures that the satellite imagery is prepared and standardized for analysis. Sentinel-2A Level-1C imagery corresponding to the study area of Roatán was downloaded from the Copernicus Open Access Hub for the years 2017 and 2025. Images were selected based on criteria of minimal cloud coverage and seasonal comparability (March to May) to reduce climatic variability and ensure consistency in land cover interpretation. To focus solely on the study area, all images were clipped to the geographic boundaries of Roatán.

Each Sentinel-2 image includes 13 spectral bands, out of which six (Table 3) were selected for processing based on their spatial resolution and relevance to land use and land cover (LULC) classification. These included Band 2 (Blue), Band 3 (Green), Band 4 (Red), and Band 8 (Near Infrared) each at 10-meter resolution; and Band 11 (SWIR 1) and Band 12 (SWIR 2), both at 20-meter resolution. These bands were chosen for their ability to distinguish between key land cover types such as vegetation, bare soil, urban surfaces, and wetlands, as supported by literature (Iurist et al., 2016).

Table 3

Spectral bands, wavelength ranges, and spatial resolutions of Sentinel-2 MSI sensor

Band Number	Band Description	Wavelength Range (nm)	Resolution (m)
B2	Blue	458–523	10
B3	Green	543–578	10
B4	Red	650–680	10
B8	Near infrared (NIR)	785–900	10
B11	Shortwave infrared 1 (SWIR1)	1,565–1,655	20
B12	Shortwave infrared 2 (SWIR2)	2,100–2,280	20

Note. Adapted from Drusch et al. (2012).

Band 2 (Blue, 458–523 nm) is especially sensitive to surface reflectance from sand, cement, and artificial surfaces, which show high reflectance in this range, while vegetation and water bodies show minimal reflectance due to chlorophyll and water absorption. Band 3 (Green, 543–578 nm) is effective for detecting vegetation vigor and identifying shallow aquatic environments. Band 4 (Red, 650–680 nm) provides strong contrast between vegetation and non-vegetated surfaces, making it essential for basic vegetation discrimination and for generating indices such as NDVI in combination with Band 8. Band 8 (Near-Infrared, 785–900 nm) captures the high reflectance of plant canopies and is critical for analyzing vegetation density and health.

Bands 11 and 12 (SWIR1: 1,565–1,655 nm and SWIR2: 2,100–2,280 nm) are particularly sensitive to surface and vegetation moisture. Their inclusion allows the detection of wetland extents and the differentiation of built-up or dry zones from moist vegetative or water-saturated areas.

The spectral reflectance curves presented in Figure 3 further illustrate how different land cover types (e.g., green vegetation, dry soil, water, concrete) respond across these wavelengths. For example, vegetation exhibits high reflectance in the NIR band and dips in the red and blue bands, while built-up surfaces and bare soils show relatively higher reflectance across the visible spectrum.

Figure 3

Spectral reflectance curves for different land surface types

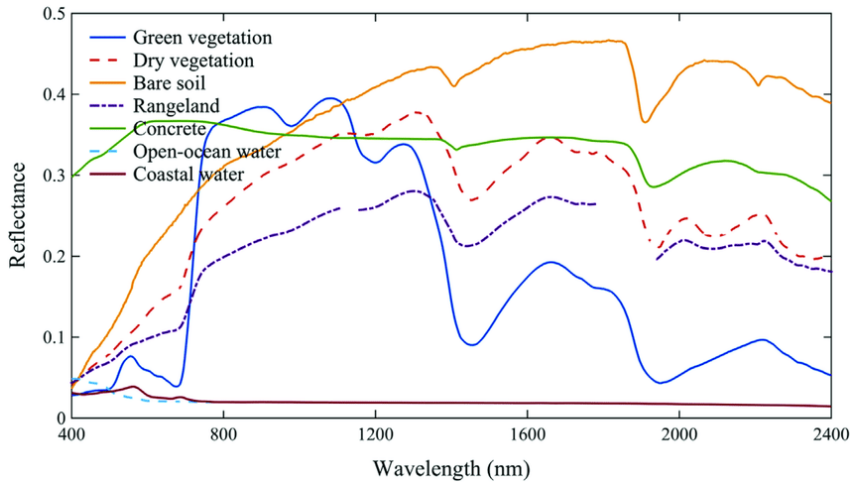

Note. Adapted from Hou et al. (2016).

The selected bands were clipped and stacked using the Semi-Automatic Classification Plugin (SCP) in QGIS® to produce a single composite raster for each year. These stacked images were used to create a true color base and enhance visualization for the selection of training samples. They also served as the foundation for defining Region of Interest (ROI) polygons corresponding to major land cover categories such as vegetation, built-up areas, wetlands, and open spaces. The resulting composite images for 2017 and 2025 are shown below in Figure 4.

Figure 4

Sentinel 2A for 2017 and 2025 respectively, followed by stacked rasters imagery

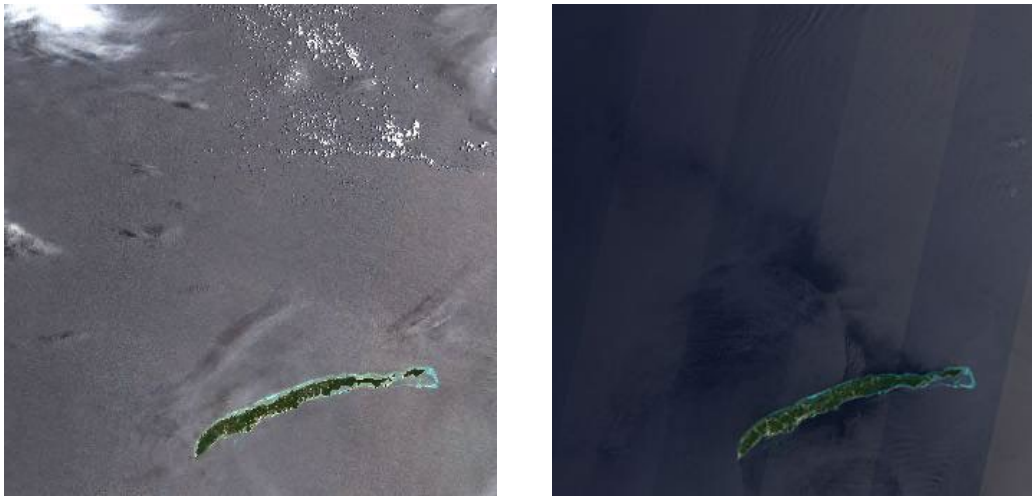

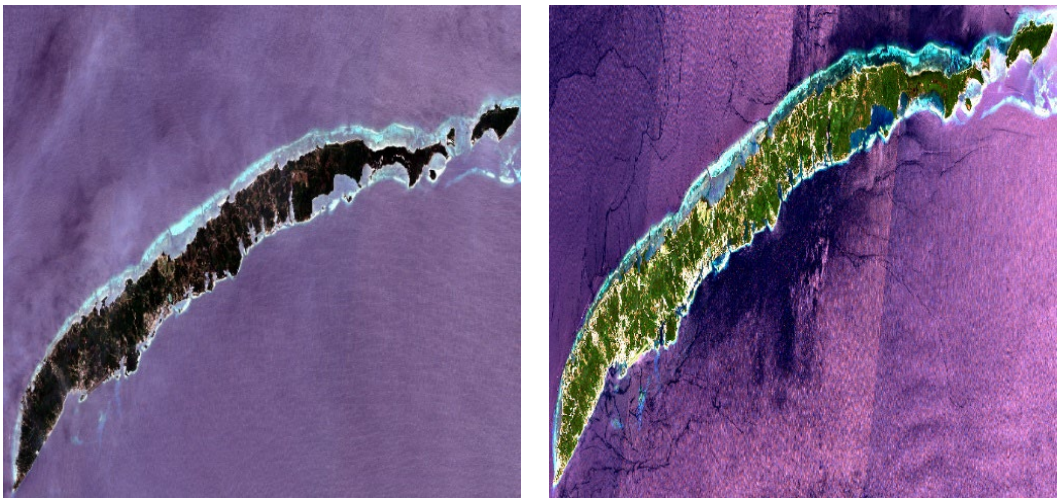

Note. Coppernicus Satellite Hub Satellite Sentinel 2A imagery

Processing phase for Supervised Classification of LULC Maps

Land use and cover was categorized into three main classes following a simplified Corine Land Cover (CLC) classification structure into subclasses (Table 4): (1) Artificial Surfaces, subdivided into Urban Fabric and Industrial, Commercial and Transport Units; (2) Forest and Seminatural Areas, including Forests and Open Spaces with Little or No Vegetation; and (3) Wetlands, with emphasis on Maritime Wetlands.

Table 4

Simplified CORINE land cover classification scheme

Level 1	Level 2
1. Artificial Surfaces	1.1 Urban Fabric
	1.2 Industrial, commercial, and transport units
3. Forest and seminatural areas	3.1 Forests
	3.3 Open spaces with little or no vegetation
4. Wet-lands	4.2 Maritime wetlands

Note. Simplified adaptation from the CORINE Land Cover classification scheme European Environment Agency (2019).

The classification process begins with the creation of training samples, also referred to as Regions of Interest (ROIs) or Training Areas. ROIs are polygons manually drawn over spectrally homogeneous areas of the image that contain pixels belonging to a single land cover class (Figure 5). These samples define the spectral signature for each class and serve as the reference input for the classification algorithm. For this study, approximately 200 ROIs were selected proportionally and

evenly distributed across the defined classes and years (2017 and 2025), ensuring representative training data for both temporal datasets.

Figure 5

Example of ROIs (Regions of Interest) in QGIS®

Note. Screenshot of polygon-based ROI definition in QGIS® during supervised classification preparation.

Using these ROIs, a supervised classification was performed through the Random Forest Mapping (RFM) algorithm, a robust machine learning method widely adopted for land cover classification used by Tuholske et al. (2017). Machine learning in remote sensing refers to a class of algorithms that learn patterns from training data to predict classifications over new data. The process involves iteratively splitting the dataset into a training set, validation set, and test set, allowing the model to calibrate, tune, and evaluate its accuracy independently (European Space Agency Lab, 2019).

The Random Forest algorithm (Figure 6) was used for supervised classification in this study due to its high execution speed, robustness to overfitting, and proven effectiveness in handling high-dimensional data. Random Forests, introduced by Tin Kam Ho (1995), are based on constructing multiple decision trees trained on randomly selected subspaces of the feature space. This ensemble

approach leverages the diversity among trees to produce more stable and accurate classifications, especially on unseen data. Unlike traditional decision trees, which often suffer from overfitting and poor generalization, Random Forests generalize better by combining the predictions of multiple diverse trees, each trained on different random subsets of the data and feature space.

A key advantage of this method lies in its ability to expand classification capacity without a significant increase in overfitting. Ho (1995) demonstrated that classification accuracy can be monotonically improved by increasing the number of decision trees, as long as the trees are sufficiently diverse. In this study, Random Forests provided a reliable framework for generating land cover maps, as they capture complex patterns in spectral data while maintaining high classification performance across different land cover classes.

Figure 6

Simplified Random Forest classification process

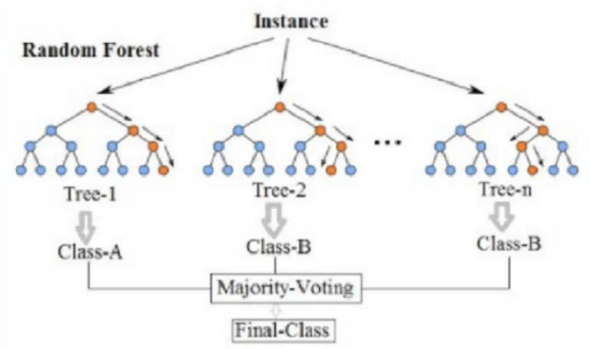

Note. Adapted from Azhari et al. (2019).

This supervised classification was performed separately for both 2017 and 2025, producing two LULC raster maps. These outputs served as the core inputs for the detection and quantification of land use/cover changes across the study period through the change detection matrix.

Postprocessing for Supervised Classification of LULC Maps

Post-processing in this study involved visual inspection, manual refinement, and accuracy validation of the classified land cover maps for the years 2017 and 2025. Rather than relying solely on automated tools such, the classification outputs were reviewed through on-screen comparison with high-resolution satellite imagery and known reference features obtained from Google Earth Pro® and local information sources. This approach enabled manual re-selection and adjustment of misclassified areas based on visual interpretation and contextual knowledge of the terrain.

Misclassifications were identified by detecting discrepancies between expected land cover patterns and the outputs generated by the supervised classification process. When inconsistencies were found—such as isolated urban pixels within vegetated zones or fragmented class boundaries, manual edits were made to improve spatial coherence and ensure that the maps more accurately represented the actual land cover distribution. These refinements were performed directly in QGIS 3.42.3® by editing raster values or updating vector-based classification masks.

Confusion Matrix

Also known as an error matrix, is a widely accepted tool in remote sensing for accuracy assessment due to its ability to detect both commission and omission errors across individual land cover classes (Congalton, 1991). The matrix (Table 5) compares the predicted classes from the classification output (rows) with known reference classes (columns), allowing for a detailed evaluation of classification performance. The structure highlights both correct and incorrect classifications: diagonal elements (e.g., a, f, k, p) indicate correctly classified pixels where the predicted and actual land cover types match while off-diagonal values represent misclassifications. Row totals reflect the area assigned to each class by the classifier, whereas column totals represent the actual number of reference area per class. The total number of evaluated area is denoted as N.

Table 5

Example of Confusion Matrix format

Classified \ Reference	Forest (*F*)	Urban (*U*)	Water (*W*)	Bare Soil (*B*)	Row Total
Forest (*F*)	*a*	*b*	*c*	*d*	R_1
Urban (*U*)	*e*	*f*	*g*	*h*	R_2
Water (*W*)	*i*	*j*	*k*	*l*	R_3
Bare Soil (*B*)	*m*	*n*	*o*	*p*	R_4
Column Total	C_1	C_2	C_3	C_4	*N*

Note: Self generated with adaptations from Congalton (1991).

In this study, the confusion matrices were generated using the Accuracy Assessment tool available in the SCP plugin in QGIS®. This tool allows the user to input validation data usually ground-truth reference points and calculates several important statistical measures.

Among them, user's accuracy (Equation 7) indicates how often the class on the map represents the real-world class; it reflects the probability that an area classified into a given category truly belongs to that category. Producer's accuracy (Equation 8), on the other hand, measures the probability that a reference area has been correctly identified by the classification; it relates to how well real features are represented on the map. Overall accuracy (Equation 9) expresses the proportion of the total number of correctly classified areas over the total number of reference areas, providing a general sense of map reliability. Kappa (Equation 10) adjusts the proportion of agreement between the classification and the ground truth (Equation 11) by subtracting the agreement that would be expected by random chance (Equation 12). A Kappa value of 1 indicates perfect agreement, 0 means no better than random, and negative values indicate worse than random.

This coefficient is particularly useful when evaluating classification quality across multiple classes and is widely considered a more conservative indicator than overall accuracy alone (Foody, 2002).

User Accuracy UA

$$UA = \frac{Correctly\ classified\ area\ in\ a\ row}{Total\ area\ classified\ in\ that\ row} = \frac{a}{R_1}, \frac{f}{R_2}, \ldots \quad [7]$$

Producers Accuracy PA

$$PA = \frac{Correctly\ classified\ area\ in\ a\ column}{Total\ reference\ area\ in\ that\ column} = \frac{a}{C_1}, \frac{f}{C_2}, \ldots \quad [8]$$

Overall Accuracy OA

$$OA = \frac{a+f+k+p}{N} \quad [9]$$

Kappa Coefficient

$$\widehat{K} = \frac{P_o - P_e}{1 - P_e} \quad [10]$$

Observed agreement

$$P_o = \frac{\sum_{i=1}^{k} xii}{N} \quad [11]$$

Expected agreement

$$P_e = \sum_{i=1}^{k} \left(\frac{R_i * C_i}{N^2}\right) \quad [12]$$

In the context of this study, all accuracy metrics were calculated using area-based confusion matrices derived from the Semi-Automatic Classification Plugin in QGIS®. This approach ensures that accuracy values reflect the actual spatial extent of each class, enhancing the relevance of the evaluation in real-world land use terms. The combination of visual inspection and confusion matrix analysis ensured that the final land cover maps were both spatially consistent and statistically reliable. Once the classifications were finalized and validated, corrected raster layers were generated to represent the land use and land cover categories for 2017 and 2025. These validated maps served as the foundation for the second phase of the study: change analysis.

Cross-Tabulation Matrix for quantification of category-level gains, losses and transitions

The cross-tabulation matrix (Figure 7), also known as a transition matrix, was used to analyze land use and land cover changes between 2017 and 2025 by comparing classifications from two time periods. This method distinguishes areas that remained stable (persistence) from those that changed, allowing for the identification of specific transitions between land cover categories. It also quantifies key components of change, including gross gains, losses, net change, and swap, providing a more detailed understanding of landscape dynamics beyond overall net change. This approach was chosen over other change detection techniques because it accounts for both the magnitude and direction of land transitions, while explicitly highlighting persistence, a common and often overlooked feature in land cover analyses. It is particularly useful for identifying systematic patterns of change that may be masked by total change summaries. The method, as formalized by Pontius et al. (2004), assumes consistent classification schemes and sufficient accuracy across time points to ensure that observed changes are not the result of misclassification. One limitation is that it does not directly account for spatial configuration or distance of change, but it lays a solid foundation for further spatial pattern analysis if needed.

Figure 7

Cross-tabulation matrix used for land cover change analysis

		Time 2			Total Time 1	Loss
		Category 1	Category 2	Category 3		
Time 1	Category 1	P_{11}	P_{12}	P_{13}	P_{1+}	$P_{1+} - P_{11}$
	Category 2	P_{21}	P_{22}	P_{23}	P_{2+}	$P_{1+} - P_{22}$
	Category 3	P_{31}	P_{32}	P_{33}	P_{3+}	$P_{1+} - P_{33}$
Total Time 2		P_{+1}	P_{+2}	P_{+3}		
Gain		$P_{+1} - P_{11}$	$P_{+2} - P_{22}$	$P_{+3} - P_{33}$		

Note. Adapted from Pontius et al. (2004).

Rows (Time 1 Categories): Represent the initial land cover classes at Time 1. These are the actual or reference categories.

Columns (Time 2 Categories): Represent the land cover classes at Time 2. These are the predicted categories.

Cells (Pij): Each cell contains a value Pij, which represents the proportion (or number of pixels/area) of the landscape that was classified as category i at Time 1 and changed to category j at Time 2.

Diagonal Values (Pii**): These values (e.g., P11, P22, P33) represent the areas that remained in the same land cover category from Time 1 to Time 2, indicating no change or persistence.

Off-Diagonal Values (Pij where i ≠ j**): These values indicate transitions between different land cover categories. For example, P12 represents the proportion of land that changed from category 1 at Time 1 to category 2 at Time 2. These highlight areas of change.

Key Components and Derived Metrics

The matrix includes totals and derived metrics that provide further insights into the nature of land cover change:

Total Time 1 (Pi+): The sum of the values in each row (Pi+) represents the total proportion (or area) of each land cover category at Time 1. This is calculated by summing across the row.

Total Time 2 (P+j**): The sum of the values in each column (P+j) represents the total proportion (or area) of each land cover category at Time 2. This is calculated by summing down the column.

Gain (P+j - Pjj**): Gain represents the net increase in the total amount of a category from Time 1 to Time 2. It is calculated as the column total (P+j) minus the diagonal value (Pjj). It shows which categories have expanded.

Loss (Pi+ - Pii**): Loss represents the net decrease in the total amount of a category from Time 1 to Time 2. It is calculated as the row total (Pi+) minus the diagonal value (Pii). It shows which categories have shrunk.

Interpreting Change Performance from Pontius Matrix

Stability Assessment (High Diagonal Values): If a particular land cover category has high values on the main diagonal (high Pii), it suggests that most of its area remained stable over the time period. This indicates a strong persistence of that land cover type.

Transition Analysis (High Off-Diagonal Values): If a particular land cover category has high values in its off-diagonal cells (i.e., large Pij values where $i \neq j$), this indicates that the category experienced significant transitions to other categories. This suggests high change dynamics.

Gain vs. Loss Analysis: Comparing the Gain and Loss values for each category helps identify which land cover types are increasing (gaining) or decreasing (losing) over the study period. This reveals trends in landscape transformation.

Results and Discussion

Spectral-Indexes: visual based analysis

The NDVI image for 2017 (Figure 8) reveals a strong presence of healthy vegetation across most of Roatán, particularly in the central and western interior zones, represented by darker green tones indicating high NDVI values (> 0.5). The coastal periphery, especially along the southern shoreline and near urbanized areas such as Coxen Hole and French Harbour, shows lower NDVI values ranging from 0.1 to 0.3, consistent with built-up land or degraded vegetation. Sparse vegetation and open areas with exposed soils are visible along roads and ridge lines, forming linear patches of lower reflectance.

Figure 8

NDVI image of Roatán for 2017 for Western portion of the island

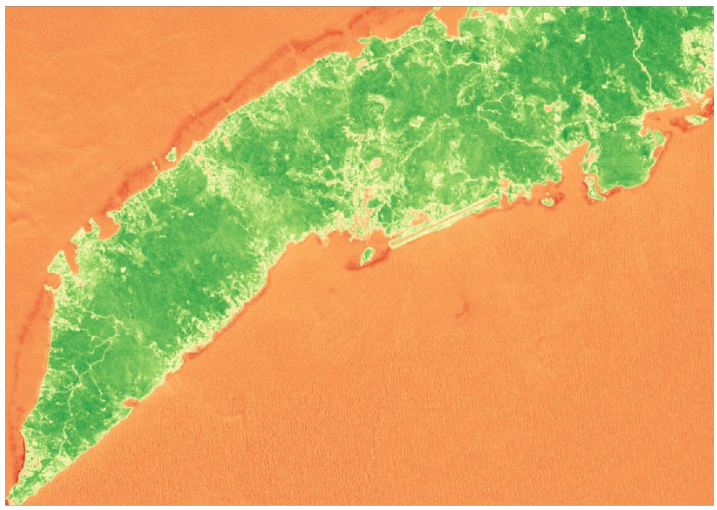

Note. NDVI map generated from Sentinel-2 imagery in QGIS®.

In contrast, the 2025 NDVI image (Figure 9) shows a subtle but notable shift in vegetation distribution. An expansion of high NDVI zones is observed in several inland areas, suggesting vegetative regrowth or increased canopy density, particularly in the northwest. However, there is also a marked increase in low-NDVI zones (red to orange), especially surrounding urban areas and transportation corridors. This indicates vegetation loss and land transformation in peri-urban zones, with previously vegetated areas being replaced or fragmented, likely due to development pressure.

Overall, the 2025 map reflects a landscape experiencing both vegetation recovery in certain natural areas and urban encroachment in formerly green zones.

Figure 9

NDVI image of Roatán for 2025 Western portion of the island

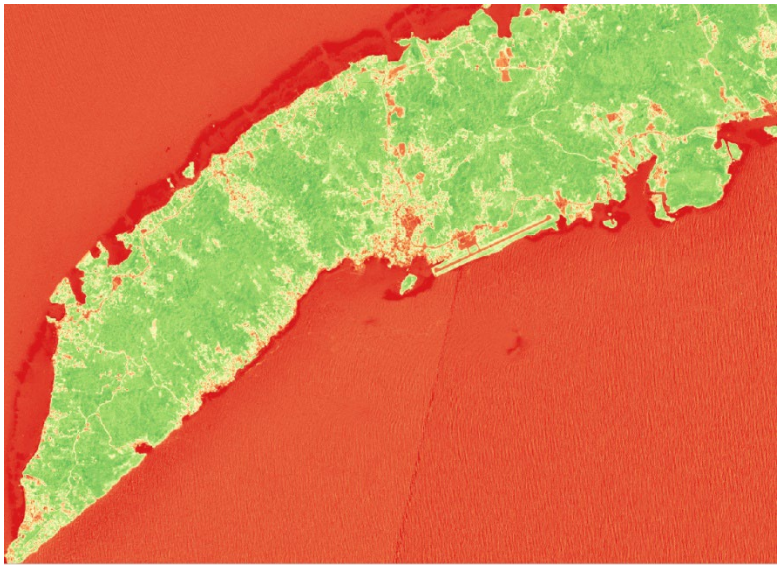

Note. NDVI map generated from Sentinel-2 imagery in QGIS®.

The NDBI images for Roatán show a noticeable increase in built-up areas from 2017 to 2025. The 2025 image (Figure 10) exhibits a broader distribution and greater intensity of higher NDBI values (represented by darker red tones), particularly concentrated around the central and western sectors of the island. These areas correspond to urban centers and zones of tourism-driven development, such as near the airport and along the coastal corridor.

Figure 10

NDBI processed image 2025 central area from south to north shore

Note. NDVI map generated from Sentinel-2 imagery in QGIS®.

In contrast, the 2017 NDBI image (Figure 11) shows a lower intensity of built-up signatures, indicating that artificial surfaces were less prevalent or less spatially extensive at that time. The lighter tone ominance in the 2017 image suggests more vegetation or natural land cover in comparison to 2025.

Figure 11

NDBI processed image of the year 2017 central area from south to north shore

Note: Self made with Sentinel 2 Imagery and the Raster Calculator from QGIS 3.42.3®.

The spatial expansion and densification of built-up areas over the eight-year period aligns with trends previously observed through the supervised classification and NDVI results. Notably, regions

that showed declining NDVI values in 2025 coincide with areas that present increased NDBI, reinforcing the interpretation that vegetation loss is being driven by urban expansion.

This transition is particularly evident in the southern and central zones near the airport and urban core, where infrastructure and development have intensified. The visual evidence from NDBI analysis supports the overall conclusion that Roatán has experienced significant land transformation, characterized by increasing urbanization and a reduction in vegetated land cover between 2017 and 2025.

Supervised Classification Land use and Land cover Maps

Figure 12 presents the supervised classification results of land use and land cover (LULC) for the island of Roatán in 2017 and 2025 using the Random Forest algorithm. The maps illustrate noticeable increases in artificial surfaces particularly urban fabric and industrial/commercial areas along the island's western and southern coastal zones. In contrast, natural covers such as forests and mangroves show signs of reduction or fragmentation. This spatial trend reflects broader patterns of land conversion observed in previous studies across Roatán, where rapid tourism-driven urbanization has replaced natural habitats, often beyond protected areas (Canty et al., 2018; Tuholske et al., 2017).

Figure 12

Supervised classification results for LULC Random Forest Classifier Algorithm maps 2017 and 2025

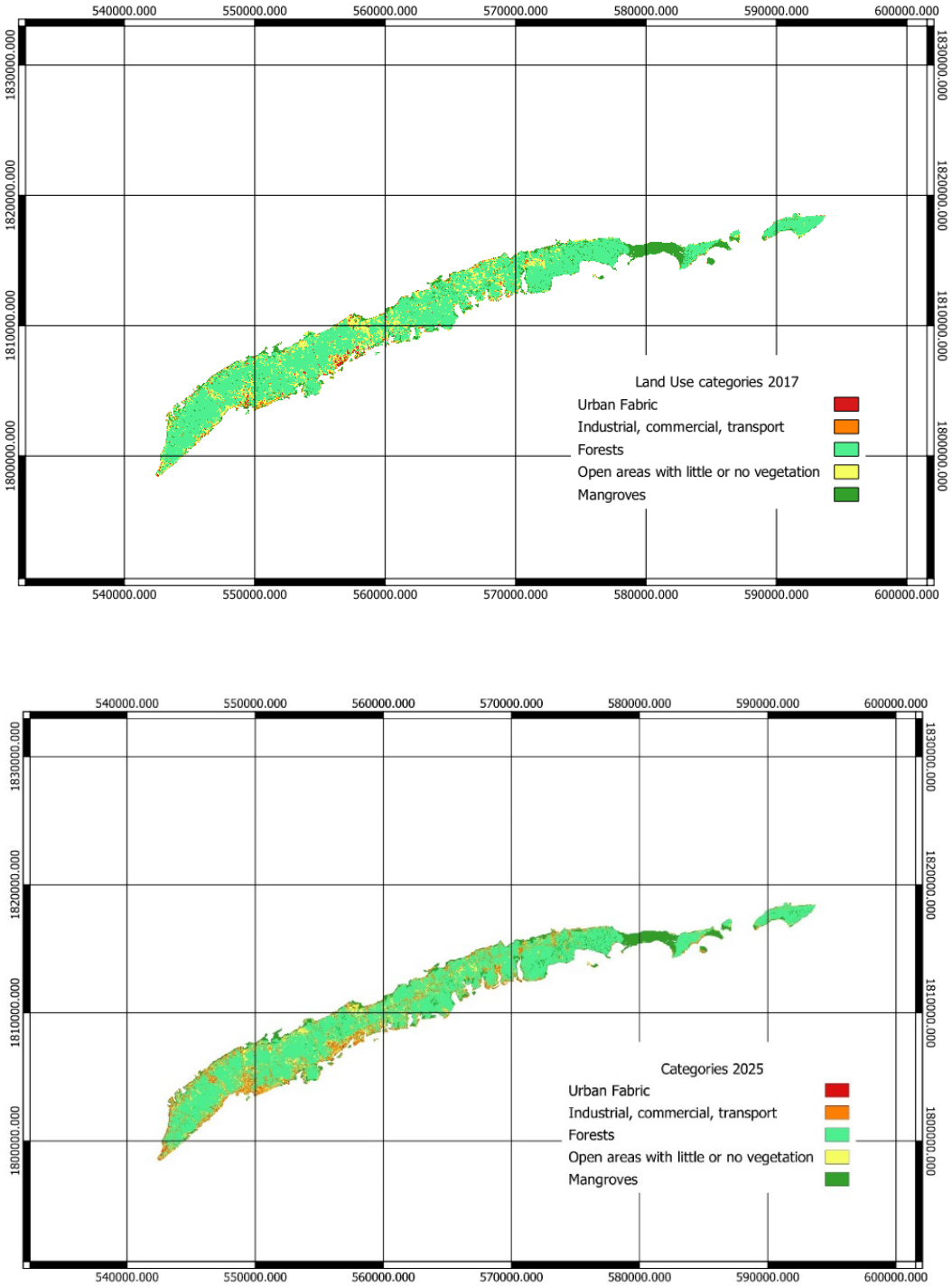

Note. 2017 top image, 2025 bottom image supervised classification performed with Random Forest using SCP Plugin for QGIS 3.42.3®.

Figure 13 shows a focused comparison of land use and land cover (LULC) in the West Bay area of Roatán between 2017 (left) and 2025 (right). A significant intensification of urban fabric and industrial/commercial zones is evident across this high-value tourism corridor. Natural covers such as forests and open vegetated spaces appear increasingly fragmented or replaced. This pattern aligns with findings by Tuholske et al. (2017), who identified West Bay as a critical hotspot for mangrove-to-urban transitions driven by unregulated coastal development. The spatial clustering of artificial surfaces in this region highlights the pressures exerted by tourism infrastructure expansion.

Figure 13

LULC images West Bay 2017 and 2025

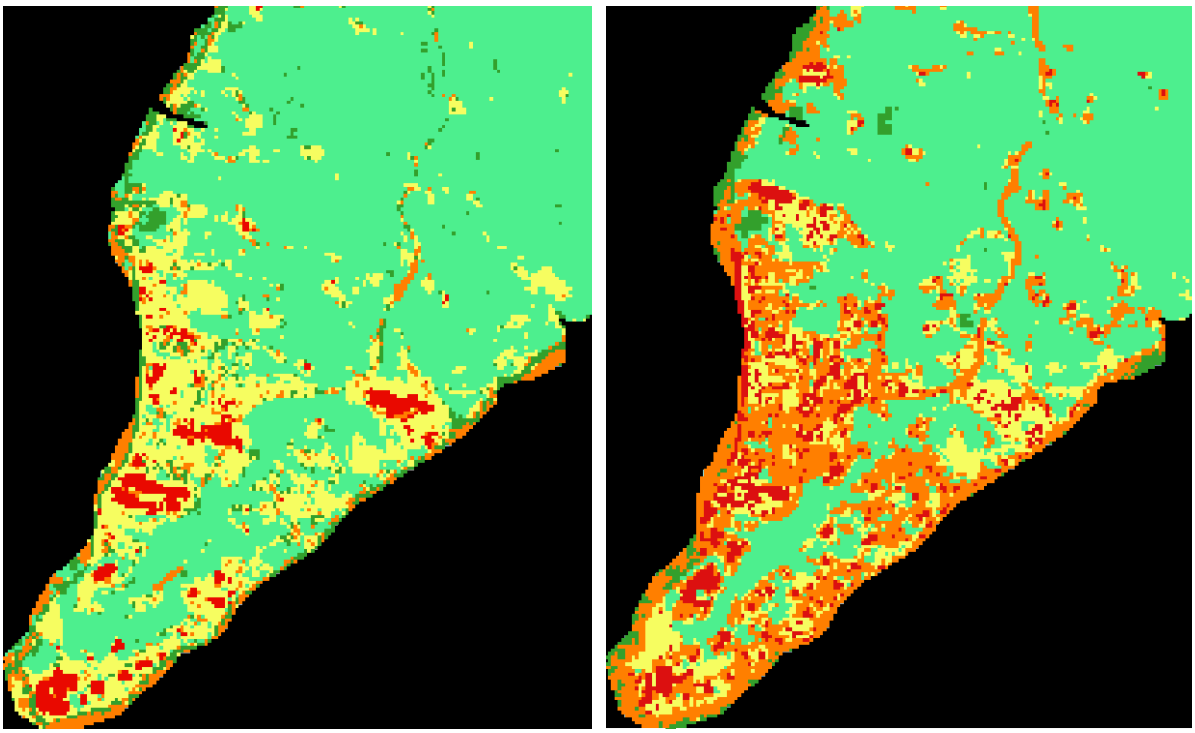

Note. 2017 left image, 2025 right image

In the Coxen Hole–Sandy Bay corridor (Figure 14), substantial urban expansion is evident between 2017 and 2025, especially around the international port, airport, and adjacent residential communities. This growth reflects the spatial pressures of tourism-driven infrastructure development concentrated around Roatán's primary gateway. According to the Roatan Tourism Bureau (2024), the island became the most visited cruise destination in Central America in 2024, receiving over 1.7 million

cruise passengers across more than 447 ship arrivals a record that underscores the island's centrality in regional tourism circuits. This surge has reinforced the need for ports, transport networks, lodging, and associated services concentrated in and around Coxen Hole.

Such intense and sustained growth aligns with regional patterns described by the Environment Department Papers (2001), who emphasize that tourism in the Caribbean frequently contributes to land conversion by stimulating induced settlement, increasing demand for infrastructure, and placing disproportionate stress on energy and water systems. Tourist-serving infrastructure often spreads beyond designated zones, especially in port hubs, accelerating land transformation in environmentally sensitive coastal corridors. The observed urbanization in Coxen Hole illustrates these dynamics, as the area has absorbed much of the island's tourism-related development, becoming a hotspot for informal and formal urban expansion as Roatán's cruise tourism continues to break arrival records.

Figure 14

LULC images Coxen hole, Sandy Bay, north and south shore 2017 and 2025

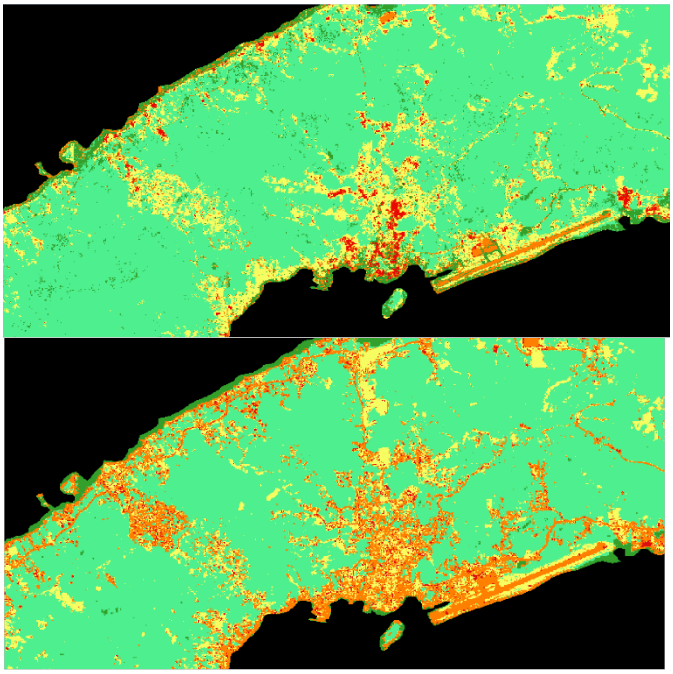

Note. 2017 top image, 2025 bottom image

The North Shore of Roatán (Figure 15) exhibits a marked increase in built-up areas between 2017 and 2025, particularly in zones previously dominated by open vegetation. This spatial shift corresponds with the expansion of key infrastructure, including the development of the landfill site, the installation of the RECO solar park, and widespread vegetation clearing in preparation for large-scale tourism investments such as the planned Margaritaville resort. The construction of the coastal road has further accelerated land conversion along this corridor. These transformations reflect a broader trend toward high-intensity land use, with long-term implications for ecological stability. As Canty et al. (2018) emphasize, such fragmentation of forest and mangrove ecosystems undermines the integrity of coastal habitats and presents enforcement challenges, especially when land-use changes outpace legal protections or institutional oversight.

Figure 15

LULC images Mud hole, north shore 2017 and 2025

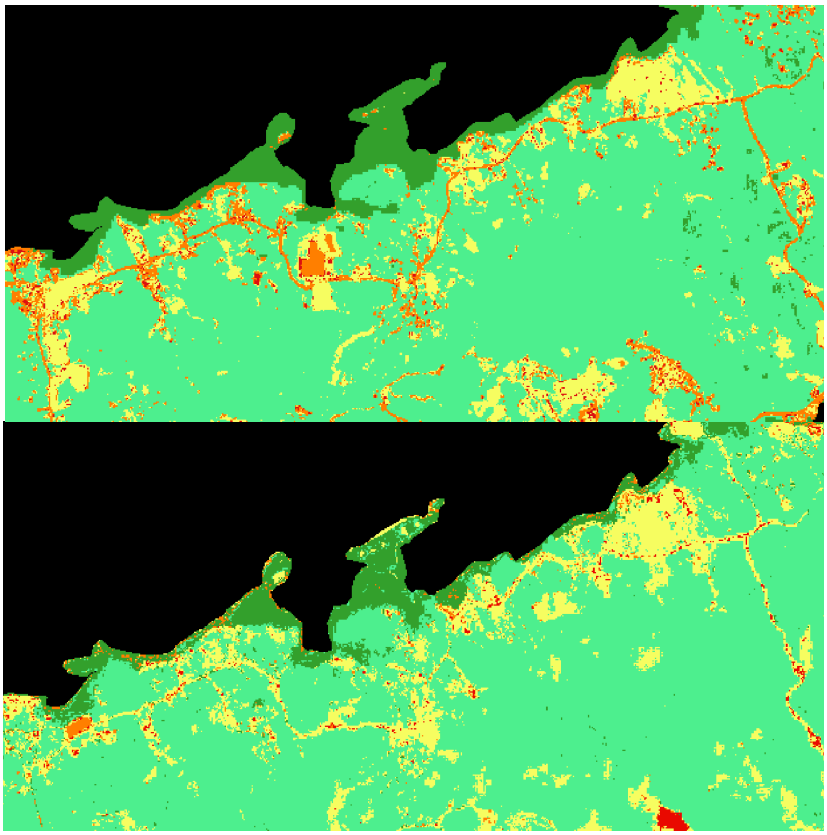

Note. 2017 bottom image, 2025 top image

Classification maps for the Crawfish and Pristine Bay area from the north shore (Figure 16) show a notable surge in urban fabric and open areas between 2017 and 2025. This transformation corresponds with major development initiatives such as the ZEDE Prospera enclave, the expansion of high-end resorts like Pristine Bay, and real estate expansion adjacent to Coral View. Previously forested and vegetated lands have been increasingly fragmented, with visible conversion into residential and commercial land uses.

These changes reflect the intensifying commodification of coastal land in Roatán driven by private investment enclaves and tourism-linked real estate speculation. As highlighted by the Environment Department Papers (2001), such tourism-induced land transformation imposes environmental pressures through increased infrastructure demands and settlement sprawl, often in areas lacking sufficient planning oversight. Without stricter ecological zoning and sustainable tourism governance, continued growth in this region risks undermining the very landscapes that attract investment and visitors.

Figure 16

LULC images Crawfish, Prospera, Pristine Bay, French Key, north shore 2017 and 2025

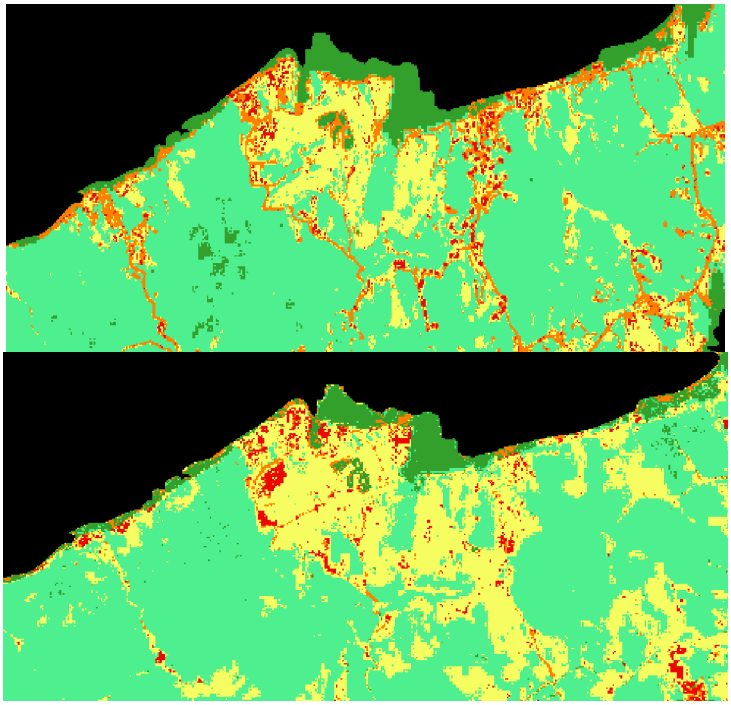

Note. 2017 bottom image, 2025 top image

The LULC classification highlights significant land transformation in the Los Fuertes and French Harbour region between 2017 and 2025 (Figure 17). Built-up areas have expanded substantially, particularly along the southern coastline, where residential development and tourism-driven infrastructure have intensified. Notable changes include the construction of RECO's solar park near the French Key area, which converted previously open and vegetated land into industrial infrastructure. In addition, the Los Fuertes community has expanded considerably, reflecting a lack of oversight and insufficient territorial planning—an issue commonly associated with unregulated tourism-driven growth in the Caribbean. Further, the progressive pavementation and extension of road infrastructure have facilitated urban sprawl inland, increasing pressure on surrounding ecosystems.

Figure 17

LULC images Los Fuertes, French Harbour, French Key, South Shore 2017 and 2025

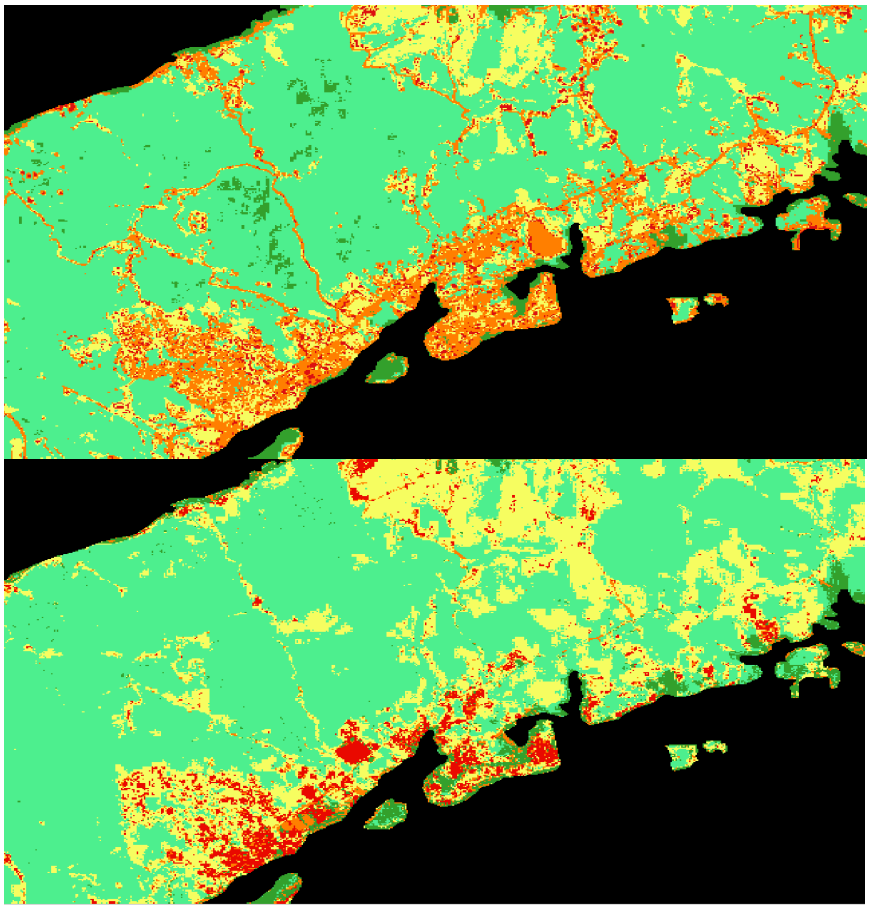

Note. 2017 bottom image, 2025 top image

The LULC analysis for José Santos Guardiola (Figure 18) reveals a contrasting trend compared to the western and central zones of Roatán. Between 2017 and 2025, there is evidence of moderate expansion of urban fabric and infrastructure, particularly along coastal corridors and road networks, but these changes are significantly less intense than in West Bay or Coxen Hole. Notably, there is visible reforestation in areas previously categorized as “open areas with little or no vegetation,” indicating land recovery processes or reduced urbanization pressure in certain inland sectors. This pattern suggests a de-intensification of urban development on the eastern side of the island, aligning with observations that development remains concentrated in the western zones where tourism and commercial hubs dominate (Tuholske et al., 2017).

While this sector has remained relatively less urbanized, the persistence of mangrove belts and vegetated zones highlights the ecological importance of maintaining current conservation strategies. (Canty et al., 2018) emphasize that these eastern ecosystems serve as critical buffers against environmental risks, and their preservation contrasts with the heavy transformation observed in Roatán's west.

Figure 18

LULC images José Santos Guardiola, east side, north and south shore

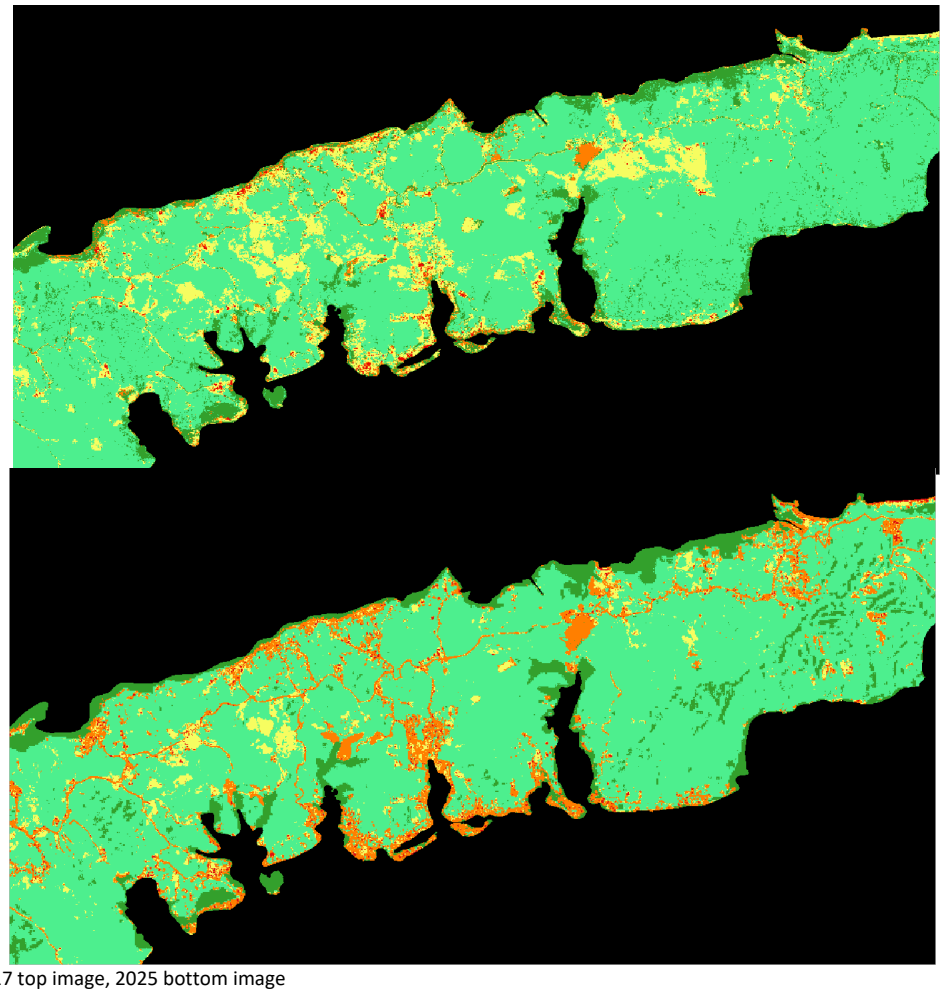

Note. 2017 top image, 2025 bottom image

This region of José Santos Guardiola (Figure 19) exhibits a markedly different pattern from the intense urbanization observed in the western zones like West Bay or Coxen Hole. The LULC maps (2017 vs. 2025) reveal a subdued urban footprint only modest growth concentrated along coastal corridors and road networks. Simultaneously, large patches of dense vegetation persist, with pockets of reforestation evident where “open areas with little or no vegetation” have regenerated. These dynamics suggest a de-intensification trend, where development pressures exist but remain limited amidst broader island transformations. Yet, the incremental encroachment through smaller roads and scattered infrastructure underscores the vulnerability of this transitional zone to future growth. Echoing Tuholske et al. (2017) findings, this pattern signals the urgent need for proactive spatial planning to preserve ecological integrity, especially given that the eastern municipality, José Santos Guardiola, houses rural communities with limited governance capacity and remain significantly less developed than the tourism-driven western half.

Figure 19

LULC images Jose Santos Guardiola, Oak ridge, Port Royal National Park, St Elena 2017 and 2025

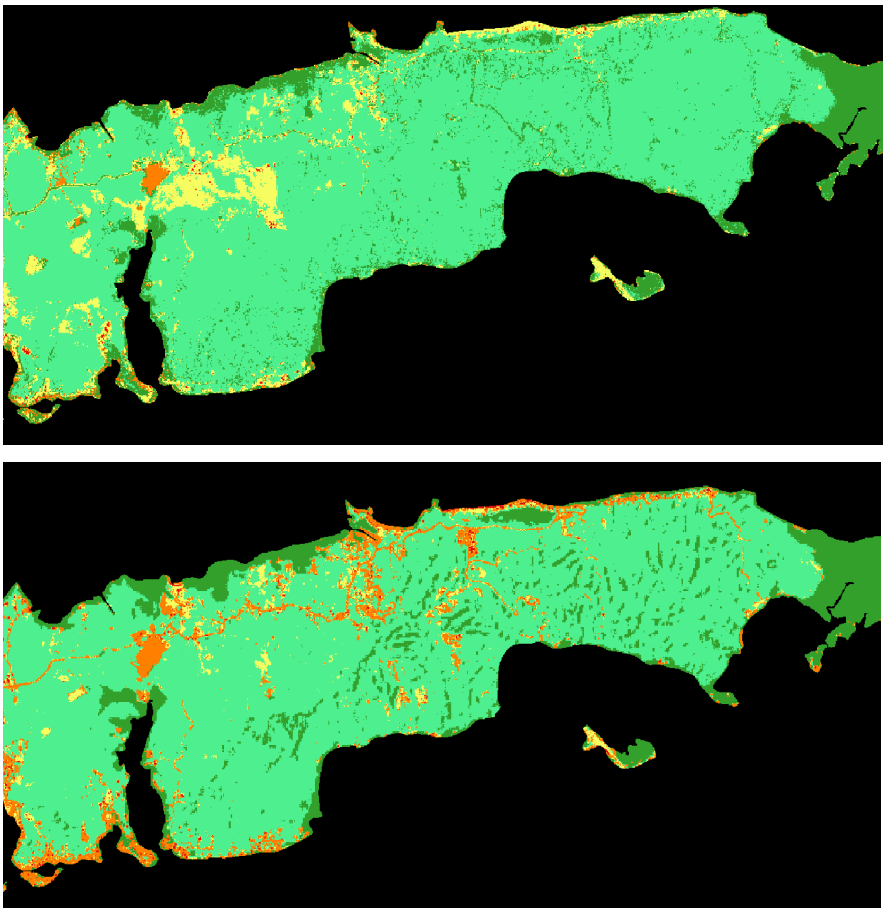

The St. Helene mangrove system (Figure 20), located on the eastern tip of Roatán, demonstrates significant ecological resilience between 2017 and 2025. The LULC classification results show minimal change, with dense mangrove coverage and surrounding forest remaining largely intact. This stability reflects its designation as part of the Bay Islands Marine National Park and its inclusion in the Ramsar Convention list of wetlands of international importance. Such legal frameworks have provided a protective buffer against the rapid urbanization and infrastructure expansion observed in western Roatán. The persistence of these mangroves is critical, as they serve not only as biodiversity hotspots but also as key buffers against coastal erosion, saltwater intrusion, and climate-driven impacts like storm surge. However, the analysis also underscores the importance of continued vigilance: although large-scale alterations are absent, incremental encroachment along coastal fringes or increased boat traffic linked to tourism could gradually erode these conservation gains if management efforts weaken.

Figure 20

LULC images St Helene mangrove system and St. Helene island, eastern side 2017 and 2025

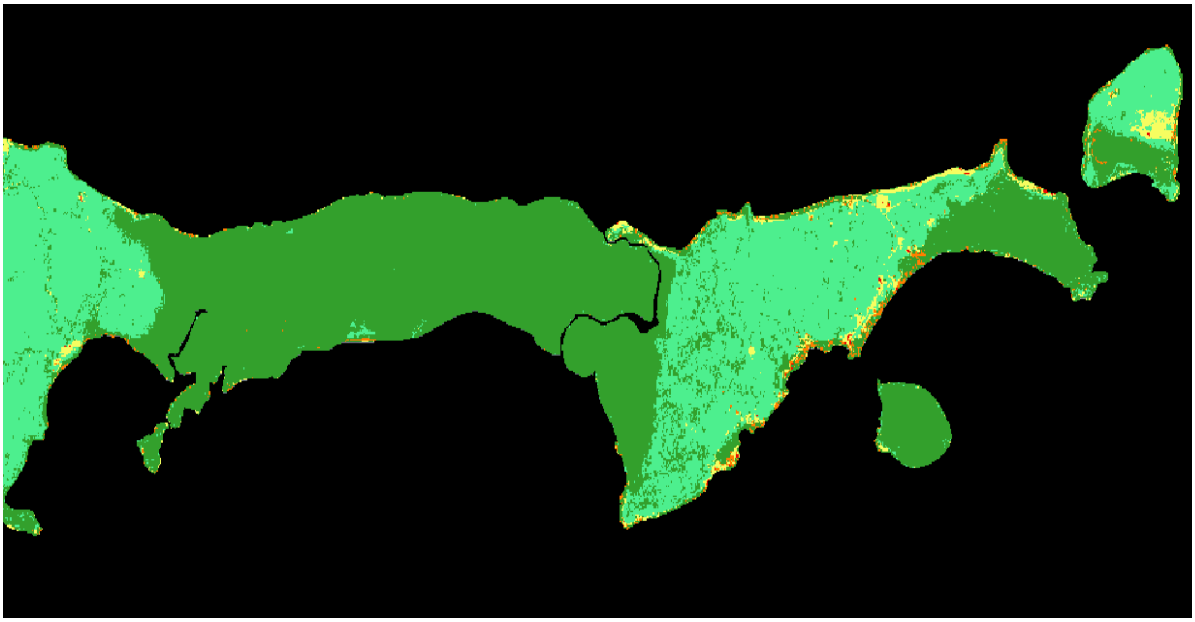

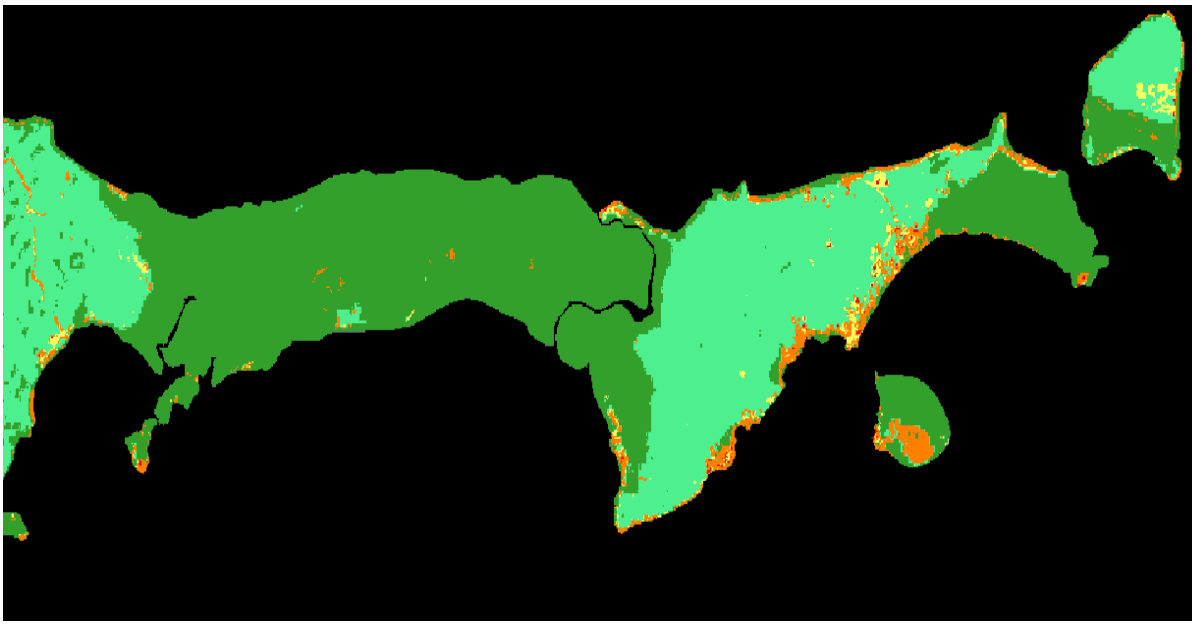

Note. 2017 top image, 2025 bottom image

Barbareta (Figure 21) presents a contrasting case of proactive conservation, where decades-long private management has safeguarded its ecological integrity. The LULC results indicate a virtually unchanged landscape dominated by dense forest and natural vegetation between 2017 and 2025, with no significant evidence of urban fabric or large-scale land clearing. This outcome reflects a deliberate strategy of private stewardship that has prioritized environmental protection while limiting development pressures. Such stability stands out in comparison to other areas of Roatán, where unregulated expansion has fragmented habitats. According to historical management reports, this privately managed island has maintained an excellent state of vegetation cover for over thirty years, positioning it as an ideal candidate for eco-tourism projects designed under sustainability principles (Valade et al., 2002). The island's combination of well-preserved ecosystems and archaeological findings enhances its potential for low-impact tourism that supports conservation objectives rather than undermining them.

Figure 21

LULC images Barbareta island, east side, 2017 and 2025

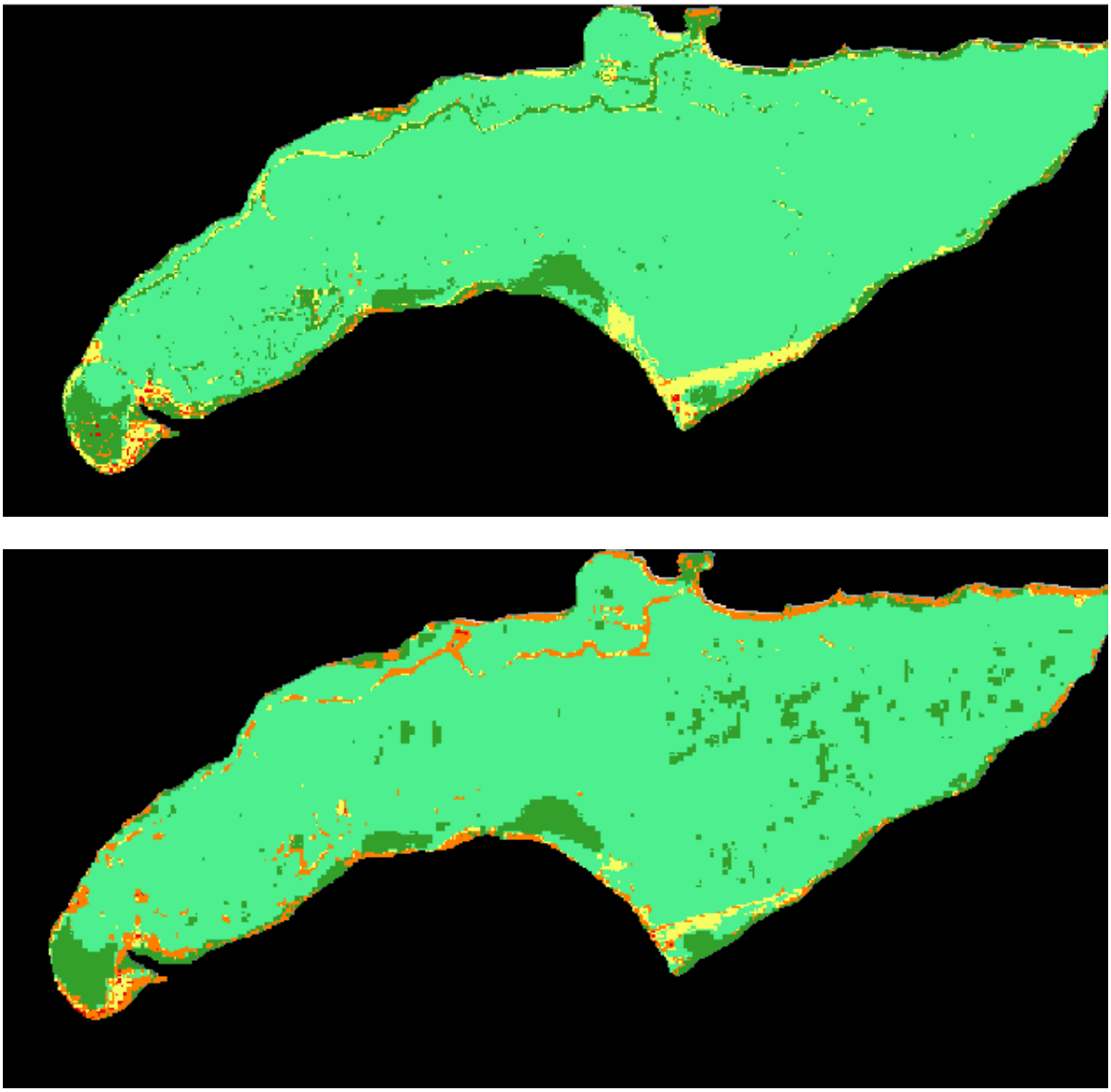

Note. 2017 top image, 2025 bottom image

Cross tabulation matrix: quantification of gains, losses, and transitions at category level

Based on the results of the Pontius Matrix (Table 6) from the random forest classification LULC from 2017 to 2025, the total losses for each land category were the following: Urban with 146.18 ha, Industrial with 160.30 ha, Forest with 1,264.37 ha, Open with 1,302.47 ha, and Mangrove with 541.86 ha. On the other hand, the total gains for each land category were the following: Urban with 196.96 ha, Industrial with 1,262.8 ha, Forest with 880.52 ha, Open with 667.44 ha, and Mangrove with 407.46 ha. As a result, the category that had the most losses of land by 2025 was the Open category, and the category that had most gains of land by 2025 was the Industrial category.

Table 6

LULC 2017 and 2025 Pontius Matrix Results Tabulated in hectares

T. 2017 | T. 2025	Urban	Industrial	Forest	Open	Mangrove	Total T1 2017	Losses
Urban	26.59	64.15	7.95	73.69	0.39	172.77	146.18
Industrial	17.42	156.19	32.78	44.53	65.57	316.49	160.3
Forest	59.34	390.34	7,891.35	311.51	303.17	9,155.72	1,264.37
Open	103.5	254.03	614.75	529.67	29.99	1,832.14	1,302.47
Mangrove	16.7	56.28	225.04	998.43	104.96	1,540.29	5,41.86
Total T2 2025	223.55	1,418.99	8,771.87	1,197.11	1,405.09	13,017.41	
Gains	196.96	1,262.8	880.52	667.44	407.46		

Note. Pontius matrix showing land cover transitions for LULC classification from 2017 to 2025 generated through SCP Plug-in

Table 7 summarizes the total extent of each land cover class for 2017 and 2025 across Roatán. The results reveal significant land use shifts over the eight-year period. Industrial land cover displays the most dramatic growth, increasing from 316.49 ha in 2017 to 1,418.99 ha in 2025—a more than fourfold rise—reflecting the rapid development of tourism-related infrastructure, energy projects, and road connectivity. This sharp growth may also be partially influenced by spectral similarity between urban fabric and industrial/commercial surfaces, which can cause overestimation in classification outputs when using pixel-based approaches.

Urban areas also show a noticeable increase, from 172.77 ha to 223.55 ha, highlighting the continued spread of settlements and service facilities linked to population growth and tourism activity. In contrast, natural covers declined during the same period. Forests decreased from 9,155.72 ha to 8,771.87 ha, a net reduction of 383.85 ha, likely due to clearing for infrastructure and tourism development in areas such as French Harbour, Pristine Bay, and the North Shore. Open areas dropped from 1,832.14 ha to 1,197.11 ha, indicating that previously undeveloped or transitional land has been converted into built-up areas. Finally, mangrove ecosystems fell from 1,540.29 ha to 1,405.09 ha, although smaller than past decades, remains ecologically critical given their role as coastal buffers. These losses point toward intensified land conversion for tourism and residential developments, particularly in zones adjacent to the north shore road, French Harbour, and West Bay corridors areas identified as hotspots for resort and infrastructure growth. Such transitions erode natural buffers, reduce aquifer recharge zones, and amplify risks of coastal erosion and saltwater intrusion, as emphasized in regional conservation studies (Canty et al., 2018).

Table 7

Results from random forest classifier for each year showing total land cover area (ha) for each land cover class for the entire island

Class	T1 2017 (ha)	T2 2025 (ha)
Urban	172.77	223.55
Industrial	316.49	1,418.99
Forest	9,155.72	8,771.87
Open	1,832.14	1,197.11
Mangrove	1,540.29	1,405.09

Note. Tabulated with data from Pontius Matrix 2017 2025

The gains, losses, and changes results (Table 8) highlight pronounced contrasts in land-use dynamics on Roatán between 2017 and 2025. Industrial land cover exhibited the most dramatic increase, with a net gain of 1,102.5 ha, representing a 348.3% change, with the highest among all categories. This surge underscores the rapid pace of infrastructure development tied to large-scale tourism and energy projects, such as the Roatan Electric Company´s solar park and resort complexes in Pristine Bay and the North Shore corridor, West Bay, etc. The considerable increase also reflects potential spectral confusion between industrial and dense urban fabric, as both surfaces share similar reflectance in high-albedo bands, potentially inflating the classified industrial category under the Random Forest algorithm.

Urban areas also recorded a substantial percentage increase (29.4%), rising from 172.77 ha to 223.55 ha, consistent with incremental settlement growth and road expansion in peri-urban and tourism-intensive zones. These patterns align with trends observed by Tuholske et al. (2017), who reported that urbanization on Roatán between 1985 and 2015 expanded by over 227%, strongly correlated with tourism-driven economic growth.

Conversely, open areas experienced the greatest proportional decline, shrinking by 34.7% (from 1,832.14 ha to 1,197.11 ha). This reduction is consistent with the functional role of these areas as transitional landscapes often cleared in preparation for future development. Their rapid conversion into urban or industrial categories reflects the early stages of construction processes that precede full infrastructure establishment. This trend emphasizes how open lands serve as “buffers” that absorb the initial impacts of tourism-related expansion, as noted in regional land-change models.

Natural covers also registered notable losses. Forest cover decreased by 4.2%, translating to a net loss of 383.85 ha, primarily through encroachment along road corridors and tourism enclaves. Mangroves declined by 8.8%, dropping from 1,540.29 ha to 1,405.09 ha. While smaller in absolute terms compared to forests and open areas, this reduction is ecologically significant, given the critical role of mangroves in coastal resilience and carbon sequestration. Tuholske et al. (2017) documented

similar dynamics, reporting annual mangrove losses of nearly 1% in unprotected areas—primarily linked to tourism infrastructure and settlement expansion—underscoring the vulnerability of these habitats despite national and international protective designations.

Table 8

Results for LULC Gains, losses, and changes

Class	Gains (ha)	Losses(ha)	Net change (ha)	% Change
Urban	196.96	146.18	50.78	29.3916768
Industrial	1,262.8	160.3	1,102.5	348.3522386
Forest	880.52	1,264.37	-383.85	-4.192461106
Open	667.44	1,302.47	-635.03	-34.66056087
Mangrove	407.46	541.86	-135.2	-8.777567861

Note. Tabulated from Pontius Matrix 2017 and 2025

Table 9 details the primary land cover transitions contributing to urbanization and artificial surface expansion between 2017 and 2025. The largest single contributor is forest-to-artificial surface conversion, totaling 449.68 ha, indicating that forested areas remain the primary source for infrastructure and settlement expansion. This reflects patterns observed in tourism-driven development corridors such as West Bay, Coxen Hole, and French Harbour, where road connectivity and resort construction have fragmented natural habitats.

Open areas to artificial surfaces account for 357.53 ha, underscoring the role of open or sparsely vegetated lands as transitional zones that are often cleared first in preparation for construction. This aligns with the substantial 34.6% decline in open areas shown in previous results, confirming their function as buffers in the development process.

Although smaller in magnitude, mangrove-to-artificial surface transitions amount to 72.98 ha, which is ecologically significant given the limited extent and critical ecosystem services provided by mangroves. This reinforces concerns raised by Rull (2023), who discussed that coastal urbanization is a key driver of mangrove loss in Roatán and the wider Caribbean.

Additionally, the matrix reveals a noteworthy forest-to-open conversion of 614.75 ha, which often precedes full urbanization. This suggests a two-stage clearing process: first reducing forest to

open land, then transitioning to artificial surfaces. Combined, these changes contribute to 880.19 ha of new artificial surfaces and 644.74 ha of open area gains, reflecting ongoing landscape restructuring toward built-up land.

Table 9

Transition trends towards urbanization

Class	Area (ha)
Forest to As	449.68
Open to As	357.53
Mangrove to As	72.98
Forest to Open	614.75
Mangrove to Open	29.99
Total Artifical Surface Gain	880.19
Total Open areas Gain	644.74

Note. Information tabulated from Pontius Mtrix LULC results

Classification Accuracy Assessment Using Confusion Matrices

The performance of the supervised land use/land cover (LULC) classifications for the years 2017 and 2025 was evaluated using area-based confusion matrices generated through the Semi-Automatic Classification Plugin (SCP) in QGIS®. These matrices compare the classified output with a set of reference data and report various accuracy metrics, including Overall Accuracy (OA), Producer's Accuracy (PA), User's Accuracy (UA), and the Kappa coefficient Congalton (1991). The results confirm the effectiveness of the Random Forest classifier (RFM) in achieving high reliability in LULC mapping, even in complex coastal environments like Roatán.

For the 2017 classification (Table 10), the model achieved an Overall Accuracy of 97.23% and a Kappa coefficient of 0.9413, indicating a very high agreement between the classified map and the reference data. Class-wise performance showed excellent reliability for Forests (PA = 99.56%, UA = 99.95%), Open Spaces with Little or No Vegetation (PA = 99.71%, UA = 88.65%), and Mangroves (PA = 100%, UA = 96.32%). Industrial, Commercial, and Transport Units also performed well (PA = 75.07%, UA = 91.16%). However, Urban Fabric exhibited the weakest performance with a Producer's Accuracy

of 33.45% and User's Accuracy of 63.70%, suggesting a significant degree of confusion with other developed land types or sparse vegetation.

Table 10

2017 Random Forest Classifier Accuracy Results

Class	Urban Fabric	Industrial	Forest	Open	Mangrove
PA [%]	33.4451	75.0676	99.5604	99.706	100
UA [%]	63.7011	91.1628	99.9486	88.651	96.3185
Kappa hat	0.6276	0.9089	0.9982	0.8703	0.9584
		Overall accuracy [%] = 97.2343			
		Kappa hat classification = 0.9413			

Note. Generated through precision assesment available in SCP Plug in for QGIS® 3.42

For the 2025 classification (Table11), the Overall Accuracy was slightly lower at 94.41%, with a Kappa coefficient of 0.8896. The classifier continued to perform strongly for Forests (PA = 98.11%, UA = 100%), Open Spaces (PA = 99.77%, UA = 63.88%), and Mangroves (PA = 99.84%, UA = 88.48%). Industrial, Commercial, and Transport Units showed improvement in both PA (77.24%) and UA (97.08%). However, Urban Fabric again remained the most problematic class, with a PA of 47.02% and UA of 59.05%, reflecting persistent spectral confusion—likely with surrounding built-up or bare areas.

Table 11

2025 Random Forest Classifier Accuracy Results

Class	Urban Fabric	Industrial	Forest	Open	Mangrove
PA [%]	47.0242	77.2411	98.111	99.7704	99.8416
UA [%]	59.0551	97.0793	100	63.8835	88.4832
Kappa hat	0.5815	0.9662	1	0.6162	0.8726
		Overall accuracy [%] = 94.4132			
		Kappa hat classification = 0.8896			

Note. Generated through precision assesment available in SCP Plug in for QGIS® 3.42

The high accuracy achieved across most classes reaffirms the suitability of the Random Forest classifier in remote sensing applications, particularly for coastal and heterogeneous landscapes. As demonstrated by Rodriguez-Galiano et al. (2012), RF is a robust ensemble learning method that consistently outperforms traditional classifiers in terms of accuracy, resistance to overfitting, and tolerance to noisy or reduced training datasets. Their study reported an average Kappa coefficient of

0.92 in complex Mediterranean landscapes using multiseasonal Landsat imagery, validating the reliability of RF-based approaches in diverse environments.

Conclusions

To compare and analyze the Land Use and Land Cover (LULC) change between 2017 and 2025, remote sensing and GIS-based techniques were applied to five different land use categories: Urban, Industrial, Forest, Open, and Mangrove. A clear difference between development and encroachment from areas previously vegetated to open and artificial surfaces. The categories that lost the most land coverage from 2017 to 2025 were Open areas with little or no vegetation, with 1,302.47 ha, and Forest with 1,264.37 ha. Both categories suffered great loss of their land for different purposes, like industrialization and urbanization.

The categories that had the most gains for land coverage from 2017 to 2025 were Industrial with 1,262.8 ha, and Forest with 880.52 ha. Both categories were positively affected in terms of having more land by 2025. The tendency for LULC was mostly inclined toward high expansion for the Industrial category and a great decrease for the Open category, followed by the Forest category, showing that industrialization had more presence on Roatán by 2025 having a negative impact over Open and Forest categories.

These observed land cover changes provide a baseline for evaluating how future land use decisions may affect ecological functions across the island. The loss of natural covers, particularly Open and Forest categories, suggests reduced buffering capacity and highlights the importance of integrated spatial planning. Continued monitoring of these patterns can support efforts to strengthen land governance and improve long-term resilience in developing zones.

Recommendations

Several recommendations are proposed to improve future land use and land cover (LULC) analyses in Roatán and similar island environments. First, it is essential to ensure a balanced and well-distributed selection of training data (ROIs) across all classes. Overrepresentation of certain categories, such as artificial surfaces, can lead to model bias and reduce classification accuracy. Future efforts should prioritize achieving representative sampling that captures the heterogeneity of land cover types on the island.

The integration of higher-resolution or multisensor data is also recommended. Sentinel-2 imagery provided a solid foundation, but limitations in spatial resolution made it difficult to distinguish between spectrally similar classes, such as dense vegetation and urban infrastructure. Incorporating higher-resolution optical imagery (e.g., Maxar) may improve class separability and enhance overall map quality. Additionally, the application of spectral indices such as NDVI, NDBI prior to classification can serve as effective filters to delineate vegetation, built-up areas, and water bodies, while also offering valuable insights into ecological trends such as vegetation recovery and urban expansion.

Optimizing classification parameters within the Random Forest model such as increasing the number of trees, enabling balanced class weights, and applying cross-validation can significantly improve accuracy and generalization. The classification algorithms complexity is limited by processing power and could have a more precise classification if the hardware allows it. Furthermore, the use of post-classification comparison methods, including the Pontius matrix, proved useful in analyzing category-level transitions and should be standard in future change detection studies. When possible, the inclusion of field-based validation or participatory mapping could strengthen classification accuracy and build local capacity for environmental monitoring.

Lastly, the observed changes in land cover patterns underscore the need for more proactive land management. It is recommended that municipal authorities use the outputs of this study to inform sustainable zoning regulations, manage urban growth, and protect remaining forested and

wetland areas. Expanding the temporal scope of future studies such as, using more frequent imagery to monitor seasonal trends would also contribute to a more dynamic understanding of Roatán's rapidly changing landscape and directly relate different factors involved in these trends.

References

Akbar, T. A., Hassan, Q. K., Ishaq, S., Batool, M., Butt, H. J., & Jabbar, H. (2019). Investigative Spatial Distribution and Modelling of Existing and Future Urban Land Changes and Its Impact on Urbanization and Economy. *Remote Sensing*, *11*(2), 105. https://doi.org/10.3390/rs11020105

Alqurashi, A. F., & Kumar, L. (2013). Investigating the Use of Remote Sensing and GIS Techniques to Detect Land Use and Land Cover Change: A Review. *Advances in Remote Sensing*, *02*(02), 193–204. https://doi.org/10.4236/ars.2013.22022

Azhari, M., Alaoui, A., Achraoui, Z., Ettaki, B., & Zerouaoui, J. (Eds.) (2019). *Adaptation of the random forest method*. https://dl.acm.org/doi/proceedings/10.1145/3368756

Burke, L. M., & Maidens, J. (2004). *Reefs at risk in the Caribbean*. World Resources Institute. http://pdf.wri.org/reefs_caribbean_full.pdf

Canty, S. W., Preziosi, R. F., & Rowntree, J. K. (2018). Dichotomy of mangrove management: A review of research and policy in the Mesoamerican reef region. *Ocean & Coastal Management*, *157*, 40–49. https://doi.org/10.1016/j.ocecoaman.2018.02.011

Carlson, R. R., Foo, S. A., & Asner, G. P. (2019). Land Use Impacts on Coral Reef Health: A Ridge-to-Reef Perspective. *Frontiers in Marine Science*, *6*, Article 562. https://doi.org/10.3389/fmars.2019.00562

Congalton, R. G. (1991). A review of assessing the accuracy of classifications of remotely sensed data. *Remote Sensing of Environment*, *37*(1), 35–46. https://doi.org/10.1016/0034-4257(91)90048-B

Da Silva, V. S., Salami, G., Da Silva, M. I. O., Silva, E. A., Monteiro Junior, J. J., & Alba, E. (2020). Methodological evaluation of vegetation indexes in land use and land cover (LULC) classification. *Geology, Ecology, and Landscapes*, *4*(2), 159–169. https://doi.org/10.1080/24749508.2019.1608409

Drusch, M., Del Bello, U., Carlier, S., Colin, O., Fernandez, V., Gascon, F., Hoersch, B., Isola, C., Laberinti, P., Martimort, P., Meygret, A., Spoto, F., Sy, O., Marchese, F., & Bargellini, P. (2012). Sentinel-2: ESA's Optical High-Resolution Mission for GMES Operational Services. *Remote Sensing of Environment*, *120*, 25–36. https://doi.org/10.1016/j.rse.2011.11.026

Environment Department Papers. (2001). *Tourism and environment in the Caribbean: An Economic Framework.* World Bank. Environmental Economic Series. https://www.researchgate.net/publication/255619697_Tourism_and_the_Environment_in_the_Caribbean

European Environment Agency. (2019). *Corine Land Cover 2018 (vector), Europe, 6-yearly - version 2020_20u1, May 2020.* https://doi.org/10.2909/71c95a07-e296-44fc-b22b-415f42acfdf0

European Space Agency Lab (Ed.). (2019). *A Machine Learning glossary*. https://philab.esa.int/a-machine-learning-glossary/

Foody, G. M. (2002). Status of land cover classification accuracy assessment. *Remote Sensing of Environment*, *80*(1), 185–201. https://doi.org/10.1016/S0034-4257(01)00295-4

Guan, D., Li, H., Inohae, T., Su, W., Nagaie, T., & Hokao, K. (2011). Modeling urban land use change by the integration of cellular automaton and Markov model. *Ecological Modelling*, *222*(20-22), 3761–3772. https://doi.org/10.1016/j.ecolmodel.2011.09.009

Hemati, M., Hasanlou, M., Mahdianpari, M., & Mohammadimanesh, F. (2021). A Systematic Review of Landsat Data for Change Detection Applications: 50 Years of Monitoring the Earth. *Remote Sensing*, *13*(15), 2869. https://doi.org/10.3390/rs13152869

Ho, T. K. (1995). Random decision forests. In Tin Kam Ho (Ed.), *Proceedings of 3rd International Conference on Document Analysis and Recognition* (pp. 278–282). IEEE Comput. Soc. Press. https://doi.org/10.1109/ICDAR.1995.598994

Hou, W., Wang, J., Xu, X., Reid, J. S., & Han, D. (2016). An algorithm for hyperspectral remote sensing of aerosols: 1. Development of theoretical framework. *Journal of Quantitative Spectroscopy and Radiative Transfer*, *178*, 400–415. https://doi.org/10.1016/j.jqsrt.2016.01.019

Instituto de Conservacion Forestal. (n.d). *Geoportal*. Retrieved August 6, 2025, from https://geoportal.icf.gob.hn/geoportal/main

Iurist, N., Stătescu, F., & Lateş, I. (2016). Analysis of Land Cover and Land Use Changes Using Sentinel-2 Images. *Present Environment and Sustainable Development*, *10*(2), 161–172. https://doi.org/10.1515/pesd-2016-0034

McBirney, A. R., & Bass, M. N. (1969). *Geology of Bay Islands, Gulf of Honduras*. https://www.semanticscholar.org/paper/Geology-of-Bay-Islands%2C-Gulf-of-Honduras-McBirney-Bass/c191f607f83d6bf299153a411094845610bf602c

Mcfield, M., Kramer, P., Álvarez, F., Drysdale, I., Rueda Flores, M., Giró Petersen, A., & Soto, M. (2018). *2018 Mesoamerican Reef Report Card.* https://doi.org/10.13140/RG.2.2.19679.36005

Pontius, R. G., Shusas, E., & McEachern, M. (2004). Detecting important categorical land changes while accounting for persistence. *Agriculture, Ecosystems & Environment*, *101*(2-3), 251–268. https://doi.org/10.1016/j.agee.2003.09.008

Roatan Tourism Bureau. (2024). *Roatan: The Most Visited Cruise Destination in Central America in 2024*. https://roatantourismbureau.com/community-updates/roatans-record-cruise-arrivals-2024

Rodriguez-Galiano, V. F., Ghimire, B., Rogan, J., Chica-Olmo, M., & Rigol-Sanchez, J. P. (2012). An assessment of the effectiveness of a random forest classifier for land-cover classification. *ISPRS Journal of Photogrammetry and Remote Sensing*, *67*, 93–104. https://doi.org/10.1016/j.isprsjprs.2011.11.002

Rull, V. (2023). Rise and fall of Caribbean mangroves. *The Science of the Total Environment*, *885*, 163851. https://doi.org/10.1016/j.scitotenv.2023.163851

Sohail, U. (2020). Analysis the Potential of Vegetation Indices (NDVI) for Land Use / Cover Classification in Karachi by Landsat 8 Data. *International Journal of Biology and Biotechnology*, *17*(2), 359–366. https://www.researchgate.net/publication/353909568

Stonich, S. C. (1998). Political ecology of tourism. *Annals of Tourism Research*, *25*(1), 25–54. https://doi.org/10.1016/S0160-7383(97)00037-6

Sutton, D. (2015). *Structural and Geophysical Analysis on Roatan Island, Honduras, Western Caribbean*. https://www.researchgate.net/publication/282669831_STRUCTURAL_AND_GEOPHYSICAL_ANALYSIS_ON_ROATAN_ISLAND_HONDURAS_WESTERN_CARIBBEAN

Tin Kam Ho (Ed.) (1995). *Proceedings of 3rd International Conference on Document Analysis and Recognition*. IEEE Comput. Soc. Press. https://doi.org/10.1109/ICDAR.1995.598994

Tomczyk, T. (2010). *Nature's refuage at Port royal: A 31-year effort of creating land protected area on the east side of Roatan, begins to bear fruit.* Bay Island Voice. http://www.bayislandvoice.com/

Tucker, C. J. (1979). Red and photographic infrared linear combinations for monitoring vegetation. *Remote Sensing of Environment*, *8*(2), 127–150. https://doi.org/10.1016/0034-4257(79)90013-0

Tuholske, C., Tane, Z., López-Carr, D., Roberts, D., & Cassels, S. (2017). Thirty years of land use/cover change in the Caribbean: Assessing the relationship between urbanization and mangrove loss in Roatán, Honduras. *Applied Geography*, *88*, 84–93. https://doi.org/10.1016/j.apgeog.2017.08.018

Valade, I., Grelot, J., & Laurent, J. M. (2002). *Proyecto manejo ambiental de las Islas de la Bahia*. https://rsis.ramsar.org/RISapp/files/36545686/documents/HN2456_ECD190603.pdf

Zha, Y., Gao, J., & Ni, S. (2003). Use of normalized difference built-up index in automatically mapping urban areas from TM imagery. *International Journal of Remote Sensing*, *24*(3), 583–594. https://doi.org/10.1080/01431160304987

Zhang, C., & Li, X. (2022). Land Use and Land Cover Mapping in the Era of Big Data. *Land*, *11*(10), 1692. https://doi.org/10.3390/land11101692

Appendices

Appendix A

Satellite Imagery for Roatan Island 2017 and 2025 from Coppernicus Data Hub

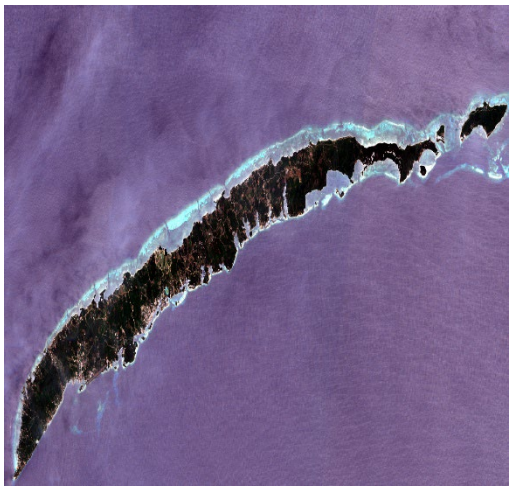

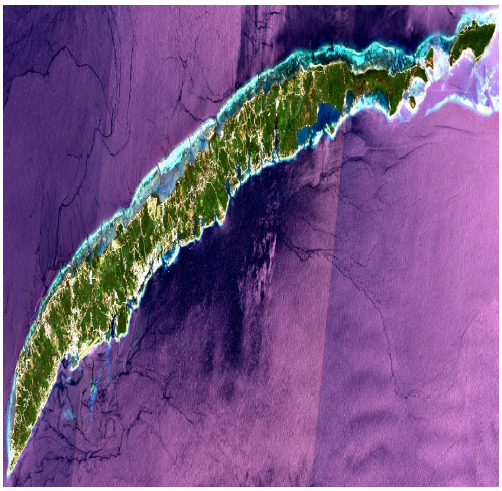

Appendix B

Pontius matrix for NDVI index classification from 2017 to 2025 (in hectares)

T. 2017 | T. 2025	Water	Artificial surface	Open spaces with little or no vegetation	Sparse vegetation	Dense vegetation	Total T1 2017	Losses
Water	135.48	11.85	1.7	0.18	0.06	149.27	13.79
Artificial surface	146.24	185.57	76.79	19.69	14.5	442.79	257.22
Open spaces with little or no vegetation	6.77	99.6	228.61	155.13	207.52	697.63	469.02
Sparse vegetation	2.92	32.87	113.19	188.36	715.83	1,053.17	864.81
Dense vegetation	5.83	70.41	147.59	236.38	10,214.47	10,674.68	460.21
Total T2 2025	297.24	400.3	567.88	599.74	11,152.38	13,017.54	
Gains	161.76	214.73	339.27	411.88	937.91		

Note. NDVI Pontius matrix showing land cover transitions and area gains/losses between 2017 and 2025.

Appendix C

2017 and 2025 Pontius Matrix

T. 2017 | T. 2025	***Urban***	***Industrial***	***Forest***	***Open***	***Mangrove***	***Total T1 2017***	***Losses***
Urban	26.59	64.15	7.95	73.69	0.39	172.77	146.18
Industrial	17.42	156.19	32.78	44.53	65.57	316.49	160.3
Forest	59.34	390.34	7,891.35	311.51	303.17	9,155.72	1,264.37
Open	103.5	254.03	614.75	529.67	29.99	1,832.14	1,302.47
Mangrove	16.7	56.28	225.04	998.43	104.96	1,540.29	541.86
Total T2 2025	223.55	1,418.99	8,771.87	1,197.11	1,405.09	13,017.41	
Gains	196.96	1262.8	880.52	667.44	407.46		

Note. Pontius matrix showing land cover transitions for LULC classification from 2017 to 2025.

Appendix D

High Res Comparison Catalog, LULC Results and Google Earth Pro®

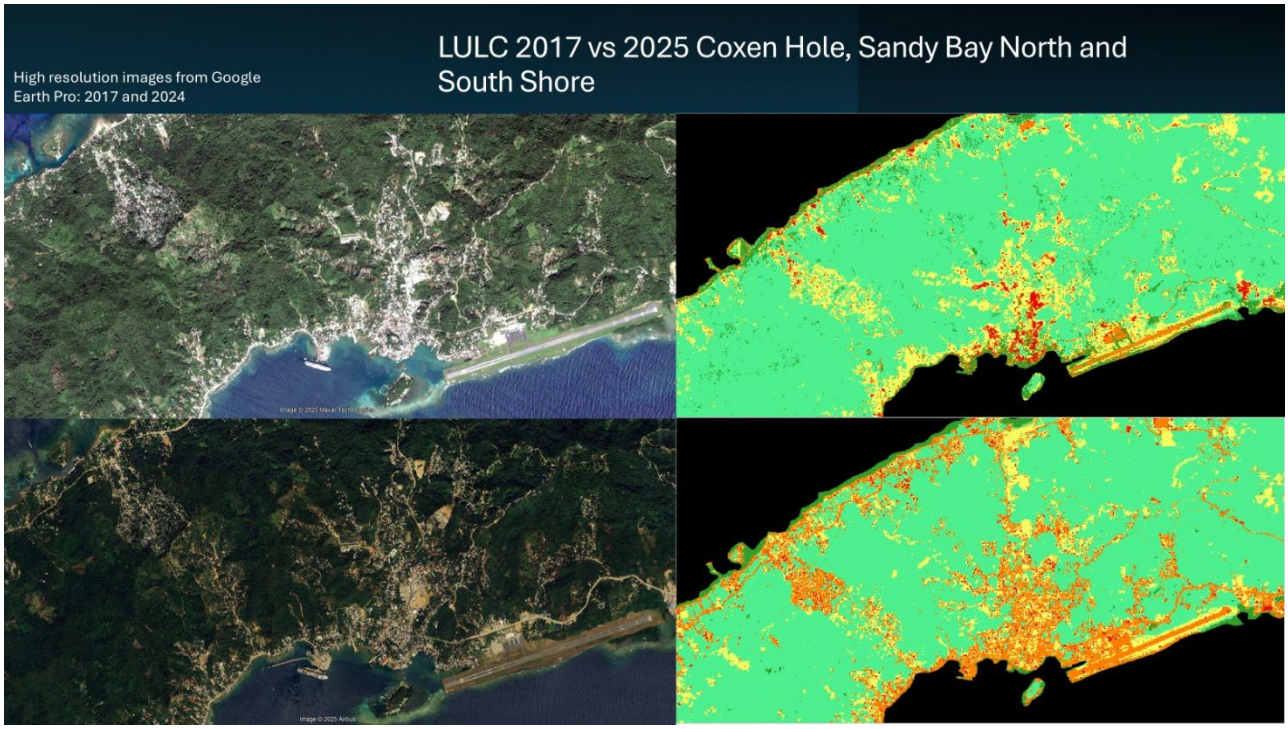

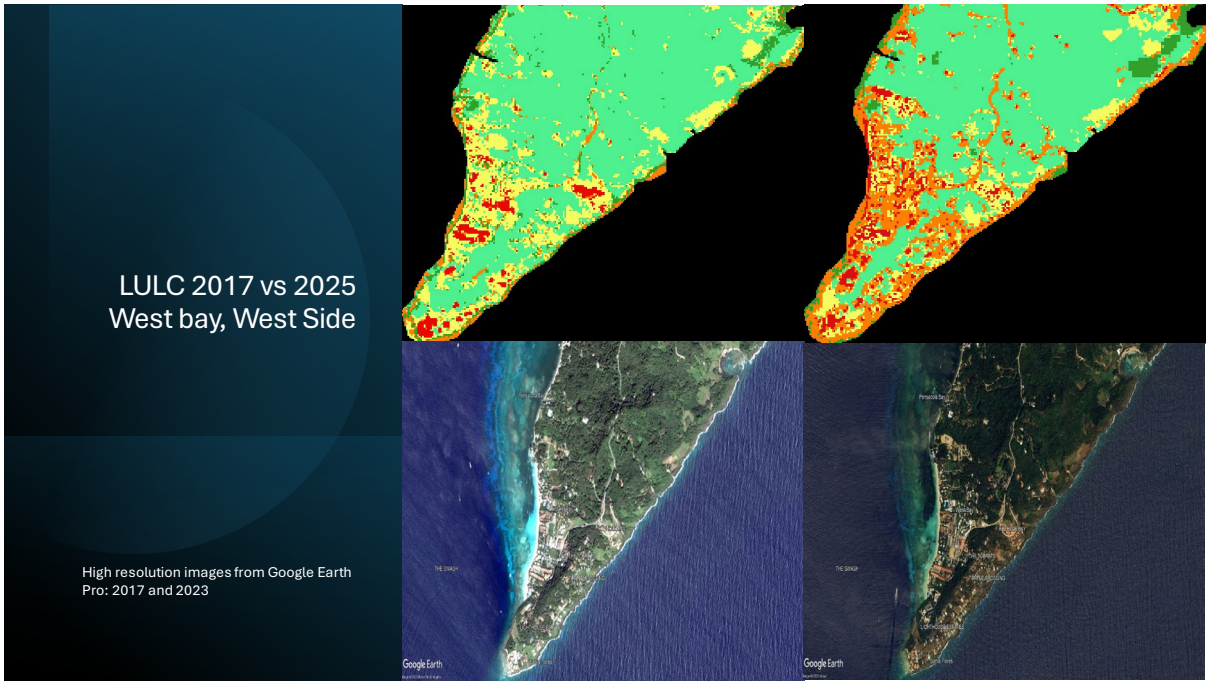

LULC 2017 vs 2025 East Side: Port Royal National Park and Camp Bay

High resolution images from Google Earth Pro: 2016 and 2023

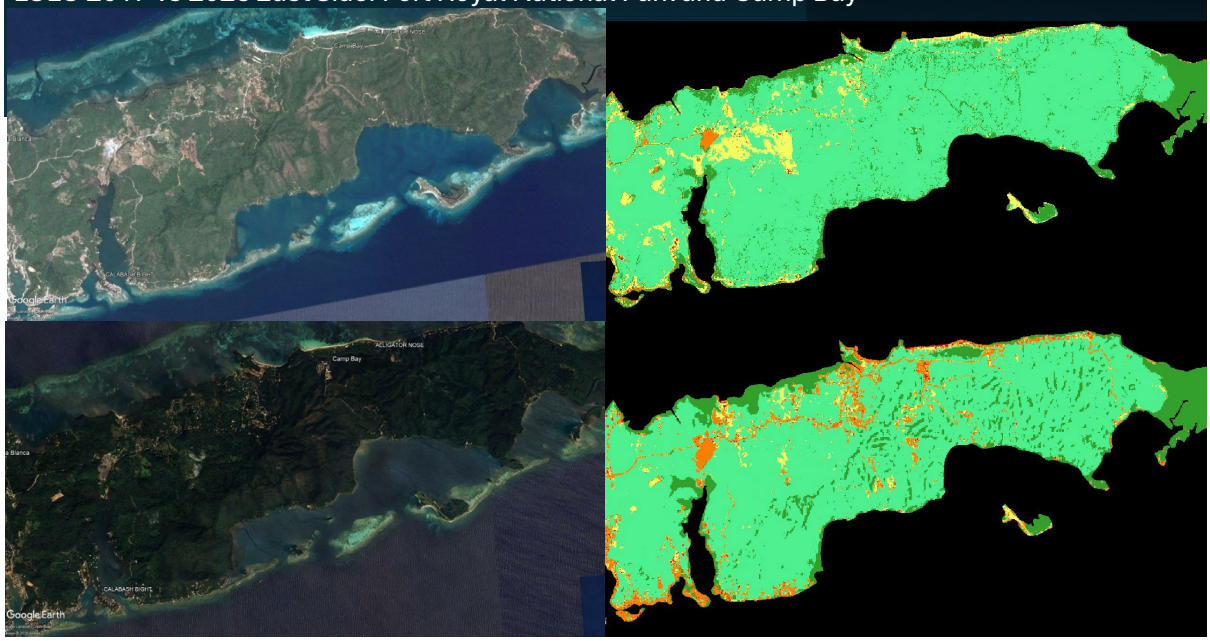

LULC 2017 vs 2025 Mud Hole, North Shore

High resolution images from Google Earth Pro: 2017 and 2024

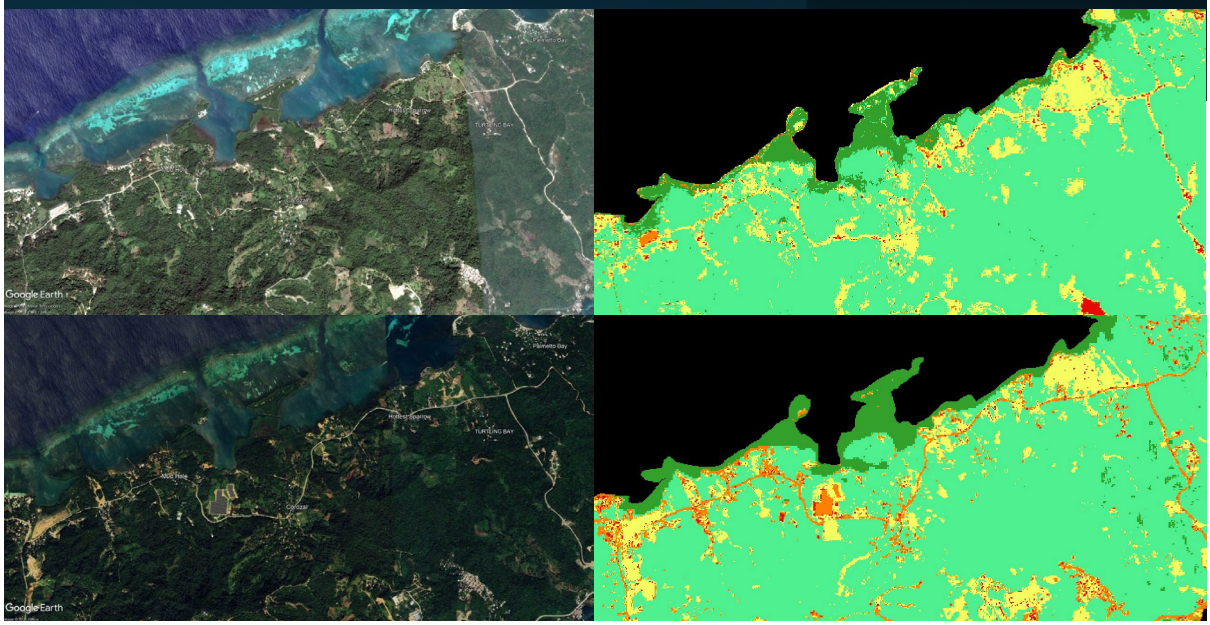

LULC 2017 vs 2025 Los Fuertes, French Harbour, French Key, South Shore

High resolution images from Google Earth Pro: 2016 and 2023

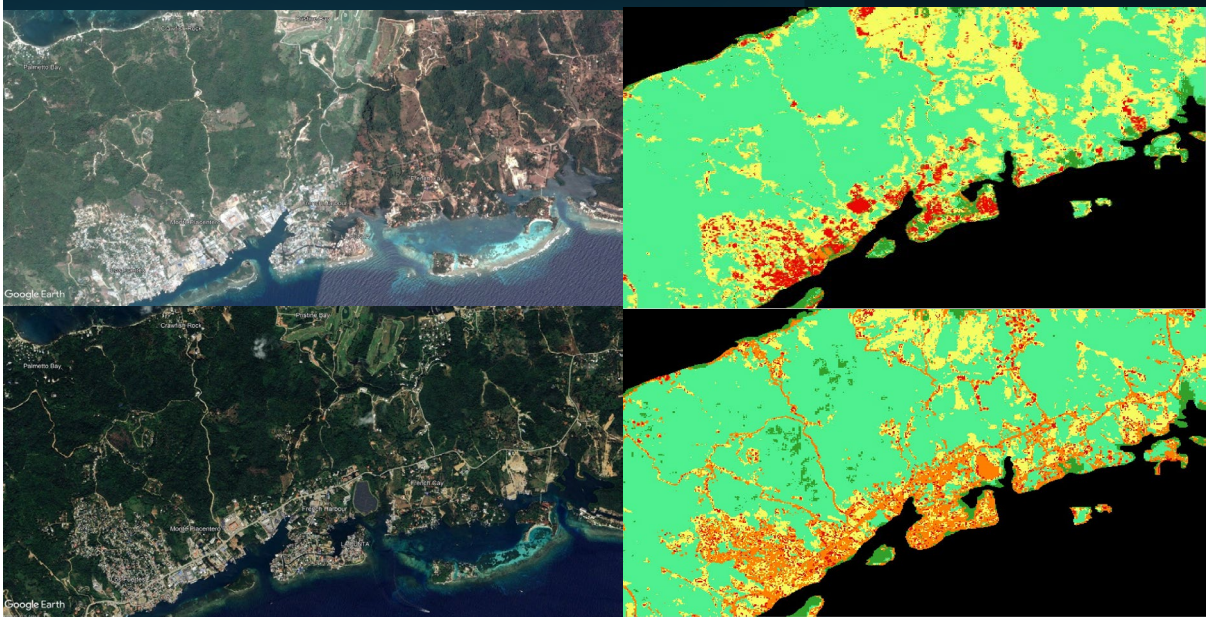

High resolution images from Google Earth Pro: 2016 and 2023

LULC Crawfish, Prospera, French Key, North Shore

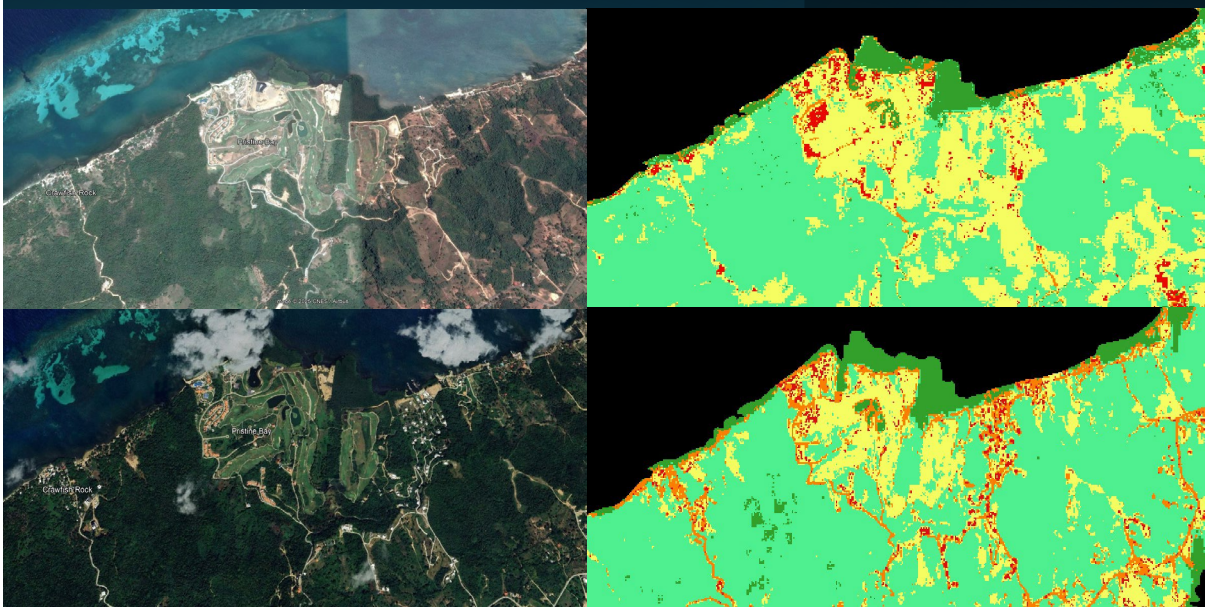

LULC 2017 vs 2025 Jose Santos Guardiola

High resolution images from Google Earth Pro: 2016 and 2023

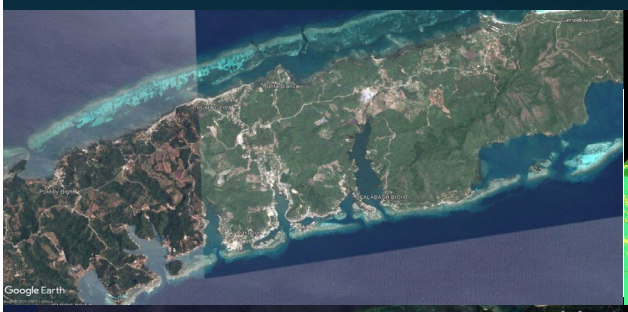

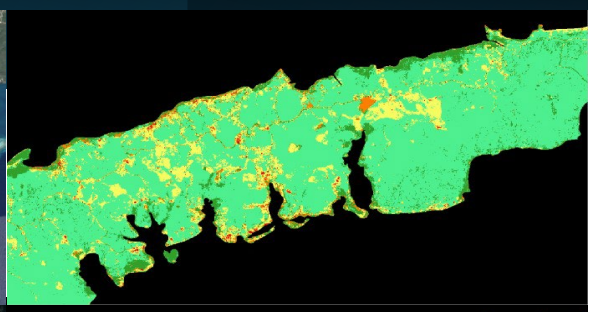

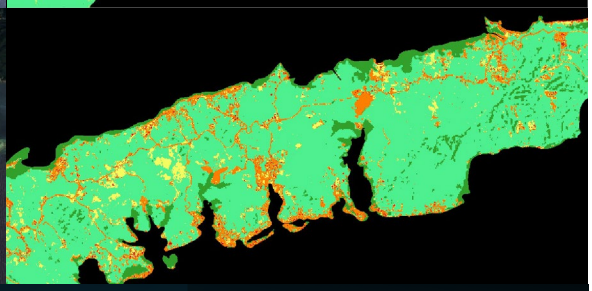

LULC 2017 vs 2025 Santa Helena

High resolution images from Google Earth Pro: 2016 and 2024

LULC 2017 vs 2025 Barbarretta

High resolution images from Google Earth Pro: 2019 and 2024